

# Hybrid Neural Network - Variational Data Assimilation algorithm to infer river discharges from SWOT-like data

Kevin LARNIER<sup>(1)(2)(3)</sup> and Jérôme MONNIER<sup>(1)(2)</sup>

<sup>(1)</sup>Institut de Mathématiques de Toulouse (IMT), France

<sup>(2)</sup>INSA Toulouse, France

<sup>(3)</sup>CS corporation, Business Unit Espace, Toulouse, France

**Correspondence:** J. Monnier (jerome.monnier@insa-toulouse.fr)

**Abstract.** A new algorithm to estimate discharges from altimetry measurements is designed for rivers with unknown bathymetry and no prior flow information. An issue in data assimilation approaches is to define a good first guess. Indeed, it is shown that if computing from the classical hydro flow models, the inverse problem may be well-defined but up to a bias (the bias scales the global estimation). This key issue is tackled by performing an artificial neural network trained on altimetric large scale water surface measurements plus a local drainage area information. The combination of this purely data-driven estimation with a dedicated algebraic flow model provides a first good physically-consistent estimation. The latter is next employed as the first guess of an advanced Variational Data Assimilation (VDA) formulation which enables to accurately capture space-time variations of the flow. For rivers belonging to the machine learning partition, the first guess value is accurate, therefore the bias of the final VDA estimation vanishes. For rivers outside the learning partition, the first guess is naturally less accurate; a bias remains. However, in this case, any mean value (eg. annual or seasonal) can be assimilated to remove it. Numerical experiments are performed for 29 heterogeneous river portions. The water surface measurements are synthetic with a 1-day repeat, corresponding to the calibration-validation orbit phase of the forthcoming SWOT mission. The estimations obtained by performing this new hybrid hierarchical inversion method are robust. They are accurate for rivers presenting features within the learning partition. For rivers far outside the learning partition, the space-time variations of discharge are accurately approximated, but potentially with a remaining bias.

## 1 Introduction

The estimation of ungauged and poorly gauged river discharges is one of the greatest challenge in hydrology. Numerous satellite missions acquire every days huge amount of data of different natures (altimetry, optical etc) which may be useful to set up river flow models, see e.g. Chen and Wang (2018) and references therein. One of the ultimate goal of river flow models is to estimate the space-time varying discharge  $Q(x, t)$ . Setting a river flow model requires to know the bathymetry, an effective friction coefficient and the (potential) lateral fluxes, see e.g. Chow (1964). The future Surface Water and Ocean Topography (SWOT) mission (NASA-CNES et al.) planned to be launched in 2022 will provide unprecedented Water Surface (WS) measurements of rivers wider than 50 – 100 m. SWOT instrument will measure the WS elevation  $Z$  (with a decimetric accuracy

25 over  $1 \text{ km}^2$ ) and the WS width  $W$  (with a varying uncertainty of a few  $m$ , depending of the river plan form). This instrument will cover a great majority of the globe with relatively frequent revisits: from 1 to 4 revisits per 21 days repeat cycle, see Rodriguez and Esteban-Fernandez (2010); Rodriguez and others (2012).

Given such WS measurements and in view to set up river flow models, the following inverse problem arises: to estimate the discharge  $Q(x, t)$  but also the unobserved bathymetry  $b(x)$  and a friction law parametrization  $K(x, t)$ . A few inversions algo-  
30 rithms to solve related inverse sub-problems have been developed, see e.g. Durand et al. (2016) and references therein where 5 different algorithms are compared on 19 river portions. The considered methods are either based on relatively basic flow models (the algebraic Manning-Strickler's law) or empirical hydraulic geometry power-laws. No method turned out to be accurate or robust in all considered configurations or regimes. All methods remain sensitive to the introduced priors e.g. a good knowledge of the bathymetry or the mean value of discharge.

35 A few data assimilation approaches based on the Kalman filter and its variants have been developed, see e.g. Biancamaria et al. (2016) and references therein.

None of them consider the complete inverse problem that is inferring the triplet  $(Q(x, t), b(x), K(x, t))$ , and not one or two of these variables only.

Two approaches based on Variational Data Assimilation (VDA) (i.e. optimal control of the flow model see e.g. Asch et al. (2016) and references therein) address the complete inverse problem that is inferring the full set of unknowns  $(Q(x, t), b(x), K)$ ,  
40 see Brisset et al. (2018); Oubanas et al. (2018b, a); Larnier et al. (2020a). In Oubanas et al. (2018a, b), the triplet of unknowns is accurately inferred from the 1D Saint-Venant flow model however the priors are computed from small Gaussian perturbations of the true values of  $K$  and  $b(x)$ . Moreover the prior defines a highly controlling rating curve  $Q(Z)$  at downstream (outflow condition). As a consequence, the inversion process converges quite easily to the correct time-dependent discharge at upstream  
45  $Q_{in}(t)$  and to the corresponding bathymetry  $b(x)$ . Indeed, the method provides the values corresponding to the imposed rating curve which is nearly exact.

The direct model elaborated in Larnier et al. (2020a); Brisset et al. (2018) and the considered inverse problem are more advanced. Saint-Venant's flow model is considered with actually unknown downstream conditions: the normal depth are imposed and are part of the inverse problem (or  $Z$  is imposed if known). Moreover this flow model is combined with an algebraic  
50 low-Froude flow model dedicated to the satellite measurements scale, see Brisset et al. (2018); Larnier et al. (2020a). This inversion strategy (HiVDI algorithm) enables to infer accurate space-time variations of the discharge but with a potential bias. Applications of the HiVDI algorithm have been instructive in different and complex contexts, see e.g. Tuozzolo et al. (2019); Garambois et al. (2020); Pujol et al. (2020). Comparison of this algorithm results with other approaches can be found in Frasson et al. (Submitted).

55

To be applied to worldwide ungauged rivers, no informed prior should be introduced in the inversions, neither in the direct model nor in the inverse method. This is one of the configuration investigated in Larnier et al. (2020a), however a potential bias on the obtained discharge estimation was remaining. This bias depends on the prior accuracy e.g. the mean value of discharge or the bathymetry elevation. To our best knowledge, no investigation have been conducted to solve the present inverse problem

60 by employing Machine Learning - Artificial Neural Network (ANN) yet. Purely-data driven estimations have been employed in hydrology e.g. in Tarpanelli et al. (2018); Chen and Wang (2018); however, these studies do not address the present challenging inverse problem: river discharge estimations from altimetry WS measurements only.

VDA-derived solutions depend on the direct model of course but also on the prior information: covariance matrix defining the employed metric(s) and the first guess value(s). The present covariance matrices are non-uniform therefore somehow  
65 physically-adaptive; they improve the robustness and the accuracy of the VDA estimations compared to those in Larnier et al. (2020a). Moreover, the first guess values are here derived from a preliminary estimation of  $Q(x, t)$  obtained from an Artificial Neural Network (ANN); the latter is trained from WS measurements and drainage area values. This first ANN estimation contributes to the definition of a good first guess value in the iterative VDA process. These new definitions of priors (plus a few other improvements of the VDA algorithm compared to Larnier et al. (2020a); Brisset et al. (2018)) enables to greatly improve  
70 the estimation's accuracy.

The resulting new HiVDI (Hierarchical Variational Discharge Inference) algorithm enables to estimate very accurately the discharge values for rivers presenting discharge values within the learning range. For rivers presenting discharges far outside the learning range, the algorithm provides estimations with a high accuracy of space-time variations but still with a potential bias. However the latter is much lower than those obtained in the previously mentioned studies; also this bias is removed if any mean  
75 value (eg. seasonal, annual) is known. Moreover past a learning period of the observed rivers (typically after one year), given newly acquired SWOT like data, the present approach provides three different estimators : the trained ANN (purely data-driven estimator), a dynamic physically-based estimator (based on the Saint-Venant equations) enabling to extrapolate both in space and time the estimations, and a low complexity algebraic flow model enabling real-time estimations.

80 This article is organized as follows. Data (altimetry type and in-situ type) and the three different scales of data and models are detailed in Section 2. Purely data driven estimations denoted by  $Q^{(ANN)}$  are analysed in Section 3, both for rivers inside the learning partition and outside the learning partition. From these estimations  $Q^{(ANN)}$ , preliminary physically-based estimations  $Q^{(0)}$  based on an algebraic flow model are obtained.  $Q^{(0)}$  constitutes the first guess value for the next step (VDA step). In Section 5, the VDA method is detailed, also the ill-posedness feature of the inverse problem is discussed. In Section 6,  
85 the physically-based estimations of  $(Q(x, t), A_0(x), K(x; h(x, t)))$  obtained by VDA are presented, both for rivers inside the learning partition and rivers outside the learning partition. Past the “calibration step” done by VDA, given newly acquired data, real time estimations  $Q^{(RT)}$  are presented in Section 7. A conclusion is proposed in Section 8. Appendix presents the rivers geometry model and the considered Saint-Venant flow model.

## 2 Data description

### 90 2.1 The altimetry and in-situ data

#### 2.1.1 The different scales

Data availability is different depending on the spatial scale. Let us detail the three different scales which are considered, see Fig. 1.

- The largest scale is the so-called “reach scale” in the SWOT scientific community, see Rodriguez and others (2012). It  
95 varies between a dozen of km to a few km ( $\approx 5$  km), depending on the river. Here it is called the SWOT Reach Scale (SwReachSc).
- An intermediate scale, called Reference Data Scale (RefDataSc), corresponds to the grid employed in the reference models (e.g. HEC-RAS) to generate the SWOT-like data and presumed true cross-sections  $A(x)$ . RefDataSc is defined by “nodes”, Fig. 1; the distance between two nodes varies between a few km to a few hundreds of meters (generally  
100  $\approx 200$  m) depending on the river.
- The Computational Grid Scale (CompGridSc) corresponds to the computational grid of the Saint-Venant flow model (see Section B). The CompGridSc elements are 100m long.

Note that a lower complexity flow model (the algebraic model presented in Section 4) will be defined at SwReachSc only.

#### 105 2.1.2 Synthetic SWOT-like data

The future SWOT instrument will provide time series ( $\sim 4 - 21$  days frequency depending on the latitude) of WS elevation  $Z$ , water extent, therefore the river width  $W$ , Rodriguez and others (2012); Rodriguez and Esteban-Fernandez (2010). These measurements will be available at different scales: at RefDataSc at the “nodes” locations and at SwReachSc when computed at the “reaches” locations. The measured WS slopes  $S$  will be accurate at large scales and therefore produced only at SwReachSc  
110 scale.

During the Calibration-Validation (Cal-Val) phase (also referred as the “science orbit”), the instrument will have a 1-day repeat orbit.

In the present study, the considered data are SWOT-like ones during this Cal-Val phase, Rodriguez and others (2012); Rodriguez and Esteban-Fernandez (2010), therefore data of the same nature as the forthcoming nominal SWOT data but with a  
115 1-day revisit. Moreover as a first step and following the Pepsi 1 and Pepsi 2 Durand et al. (2016); Frasson et al. (Submitted) benchmarks design (Discharge Algorithm Working Group of the SWOT Science Team), we consider perfect data. The next phase will consist to introduce realistic noises; the last phase consists to consider outputs from the SWOT Science simulator or data from AirSWOT (AirBorne) campaigns. This scientific approach enables to rigorously analyse the methods capabilities (or not) to tackle the present ill-posed inverse problem.

120 Future works will be dedicated to real SWOT-like data with realistic errors and temporal samplings; for instance, data computed using the SWOT Science Instrument simulator or acquired during a AirSWOT (airborne) campaigns. Note such study using the former version of HiVDI algorithm (VDA based only) has been conducted in Tuozzolo et al. (2019).

Here the considered data are as follows:

- 125
- The complete set of measurements  $(Z_{r,p}, W_{r,p}, S_{r,p})$  at SwReachSc for each reach  $r$  and at each instant  $p$ .
  - The measurements of  $(Z_{r,p}, W_{r,p})$  at RefDataSc for each “node”  $r$  and at each instant  $p$ .

In the sequel and if ambiguous, it will be clarified at which scale the different fields and data are considered.

The SWOT instrument should provide WS measurements  $(Z, W)$  at the “node scale” 200m long. This fine scale data is represented by data available in the Pepsi 1 and Pepsi 2 databases at RefDataSc.

130 Each river portion is decomposed into  $R$  reaches:  $r = 1, \dots, R$ , Fig. A1. It is assumed that  $(P + 1)$  instants of measurements are available; the corresponding measurements are ordered by flow elevations  $Z$ ; the case  $p = 0$  denotes the lowest water level and  $p = (P + 1)$  denotes the highest.

Given a river portion, the resulting SWOT data set is  $\{Z_{r,p}, W_{r,p}\}_{R, P+1}$  plus WS slope  $\{S_{r,p}\}_{R, P+1}$  at SwReachSc.

135 Depending on the considered flow model, the  $r$ -th “spatial point” denotes either the node or the reach number. More precisely, the node scale is the adequate scale for the Saint-Venant flow model B1, while the larger reach scale is consistent with the low complexity algebraic model 5, see Garambois and Monnier (2015); Brisset et al. (2018) for investigations.

Note that SW elevations  $Z$  may be obtained from multiple altimetry missions databases, see eg. DAHITI database Schwatke et al. (2015), however at heterogeneous accuracy and frequencies; also, rivers width  $W$  may be extracted from eg. the Global  
140 With Database built in Yamazaki et al. (2014).

Finally, let us point out that if considering the nominal SWOT orbit (21 days repeat orbit) with realistic noise, the scientific challenge which consists to solve the considered inverse problem remains of same nature as the present one; of course with higher uncertainties and a time limitation of the discharge estimations (see details at the end of next section).

145

### 2.1.3 Synthetic in-situ data

### 2.1.4 References data: Pepsi datasets

To generate synthetic data of discharges, we employ the Pepsi databases which have been built up for the Pepsi 1 and 2 challenges, see Durand et al. (2016); Frasson et al. (Submitted). These databases are a compilation of synthetic flow observations  
150 generated from outputs of various hydraulic flow models. These models have been calibrated. It is assumed by the Discharge Algorithm Working Group of the SWOT ScienceTeam that these models represent sufficiently well the flow to constitute

references for benchmarking discharge algorithms, Durand et al. (2016); Frasson et al. (Submitted). The present SWOT like observations have been generated from these flow models outputs at daily sampling (corresponding to the CalVal orbit phase), both at RefDataSc and at SwReachSc (see previous paragraph). For the aforementioned reasons, here no errors have been added to the models outputs.

They contain numerous river portions with various hydro-geomorphological properties and various regimes. Other more sophisticated datasets exist (SWOT Instrument Simulator, AirSWOT campaigns data, see e.g. Tuozzolo et al. (2019), but they are restricted to very few river portions only. As a consequence, such datasets are not well suited for machine learning experiments.

The number of days, nodes and reaches varies from one river portion to another. The number of days varies from 12 days to a full year. The number of nodes by river portion varies from 21 to 3189; the number of reaches varies from 4 to 16. Some of the river portions in this dataset were outside the range of SWOT visibility since the width was less than 50m; they were then removed from the dataset. Similarly river portions with less than 100 days of observations were removed. Finally, a total number of 29 river portions were selected which represents a total count of 145 reaches and (time multiplied by space) of 55 525 observations of any variable at SwReachSc. At RefDataSc, values of  $(Z, W)$  and  $(Q, A)$  are available. At SwReachSc, values of  $(Z, W, S)$  and  $(Q, A)$  are available.

### 2.1.5 Ancillary data

To train the ANN, we will use local drainage area values (denoted by  $\mathcal{A}$ ) as an input variable. In the present altimetry context, this variable may be considered as an ancillary data. The knowledge of  $\mathcal{A}$  will be the only prior of the forthcoming inversion algorithm.

Values of  $\mathcal{A}$  is extracted from HydroSHEDS (Hydrological data and maps based on SHuttle Elevation Derivatives at multiple Scales), Lehner et al. (2008). This database is a collection of geo-referenced datasets (vector and raster) at various scales (from 3 arc seconds to 30 arc seconds). It includes river networks, void filled DEM, watershed boundaries, drainage directions and flow accumulations. As the flow accumulation in HydroSHEDS is expressed in number of cells, a dedicated script to compute drainage area (flow accumulation in m<sup>2</sup>) from the drainage directions has been developed. Then the drainage area  $\mathcal{A}$  at every reach  $r$  of the PEPSI database has been computed using the geo-location of every river portions.

## 2.2 Statistic description of the datasets

Data representing the important features of the considered rivers portions are presented in Fig. 2. More precisely for each river portion are presented the mean value, quartiles (and outliers) for the discharge  $Q$  and width  $W$ , Fig. 2 (Top). The drainage area  $\mathcal{A}$  (km<sup>2</sup>) related to the considered river portion is also plotted, Fig. 2 (Bottom). This variable is not present in the flow models however it is an important information to estimate discharges using the ANN (see next Section).

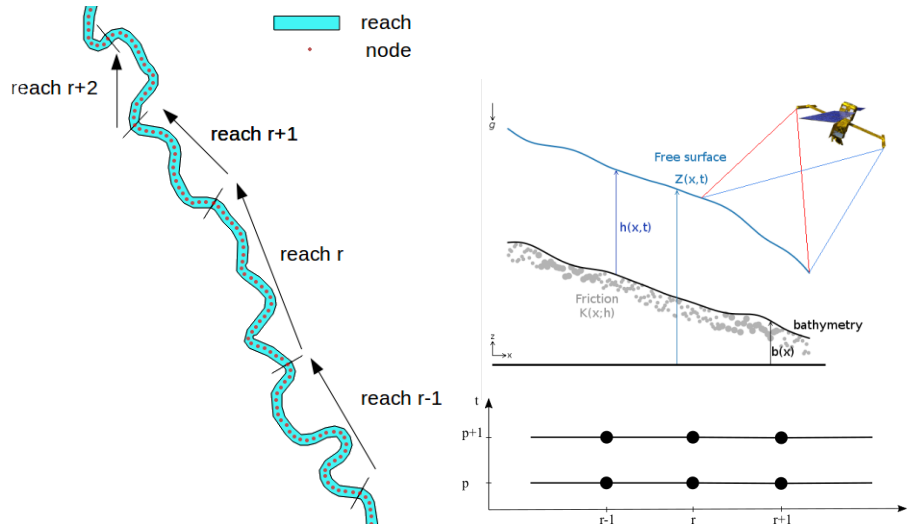


**Figure 1.** (Left) Top view of an observed river with the two different scales SwReachSc and RefDatSc.

At each reach  $r$  (cyan polygons, Swot reach) corresponds a set of WS measurements  $(Z_{r,p}, W_{r,p}, S_{r,p})$ . The algebraic (low complexity) flow model is solved at this scale.

At each node (red circle, RefDatSc) corresponds a presumed true cross-section  $A_r$  and a set of WS measurements  $(Z_{r,p}, W_{r,p})$ .

At CompGridSc points (not shown here,  $dx = 100m$ ), no SWOT like data is available. The Saint-Venant flow model is solved at this scale.

(Right)(Top) The inverse problem: inferring the flow discharge  $Q(x,t)$  ( $m^3/s$ ), the bathymetry  $b(x)$  ( $m$ ) (equivalently the unmeasured lowest wetted cross-section  $A_0(x)$ , see also Fig. A1) and an effective friction parameter  $K(x,t)$  from WS measurements  $(Z, W)(x,t)$ .

(Right)(Bottom) Space-time grid of the observations: reach number  $r$  in  $x$ -axis, satellite overpass instant  $p$  (re-ordered from low to high flowline) on the  $y$ -axis.

185 Three rivers (Jamuna, Mississippi downstream and Padma) present particularly high values of discharges and widths (as well as high values of drainage area  $\mathcal{A}$ ). It can also be noted that the Missouri river portion presents high values of drainage area.

This analysis helps to set up a-priori pdf and covariance kernels to solve the algebraic flow (Section 4.3) and the VDA optimization problem (Section 5.2).

190 The Pearson correlation coefficient  $R^2$  has been computed between numerous variables:  $Z$ ,  $W$ , elevation variations  $dZ$ , wetted crossed-sections variations  $dA$  (both being computed between two ordered overpasses), also soil composition (percentage of clay, sand and silt), mean annual rain, mean annual temperature and land use (numerical results not presented). The only high correlations are between:  $(Q, dZ)$ ,  $(Q, dA)$  (hence somehow  $(dA, W)$  too) and  $(Q, \mathcal{A})$ .

### 2.3 Learning set $Q$ -Lset and assessment sets ( $Q$ -Vset-in, $Q$ -Vset-out)

195 The learning dataset employed in this section is constituted by river portions presenting mean discharge value lower than  $10\,000 m^3/s$ , see Fig. 2 (Top Left). All river portions satisfying this criteria are considered except 4 of them (which have been

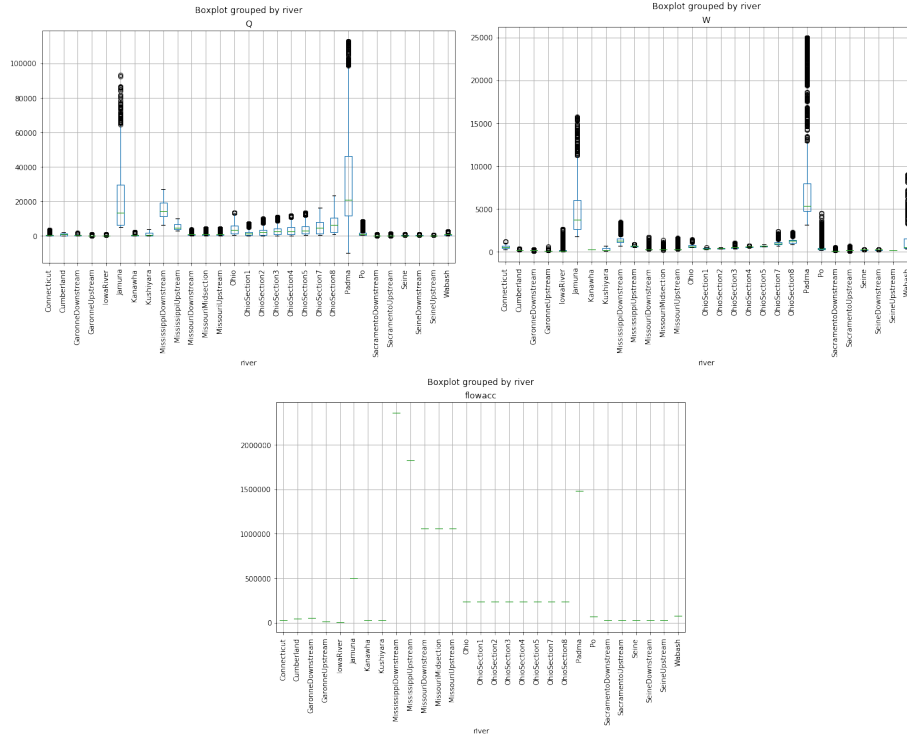


**Figure 2.** Hydraulic features of the considered river portions. The green bar indicates the mean value, boxes indicate  $\pm 25\%$  quartiles, circles are outliers (Python boxplot command). (Top Left) Discharge  $Q$  ( $m^3/s$ ). (Top Right) Width  $W$  ( $m$ ). (Bottom) Drainage area  $A$  ( $km^2$ ).

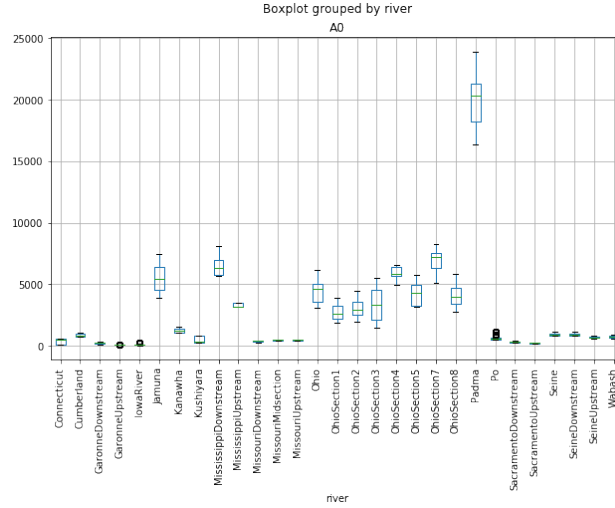


**Figure 3.** Values of the lowest wetted cross-section  $A_0$ .  $A_0$  is an unobserved quantity.

randomly chosen for validation). The resulting learning set is denoted by  $Q$ -Lset. It contains data related to  $(24 - 4) = 20$  river portions. This corresponds to a total of 41 747 “training examples” of 4 predictor variables:  $(dA, W, S, \mathcal{A})$  plus one target variable ( $Q$ ) for each observation location and each overpass.

200 The remaining 4 rivers portions in the  $Q$ -Lset are: Garonne downstream, Missouri mid-section, Iowa and Ohio. They constitute the validation dataset; it is denoted by  $Q$ -Vset-in.  $Q$ -Vset-in will be used to assess the prediction capabilities of the trained ANN (Section 3). The obtained results will show the estimation capabilities of the trained ANN for rivers presenting values of  $Q$  within the learning range (hence the name  $Q$ -Vset-in).

In other respect, the rivers portions presenting discharge values greater than  $10\,000\text{ m}^3/\text{s}$  (Jamuna, Mississippi downstream and Padma, see Fig. 2 (Top Left) are gathered in the dataset denoted by  $Q$ -Vset-out.  $Q$ -Vset-out will be used to assess the estimation capabilities of the trained ANN for rivers presenting values of  $Q$  outside the learning range.

## 2.4 On the choice to define two river classes: $Q$ -Lset and its complement

The preliminary statistical analysis show that the great majority of “examples” (in the sense of machine learning) presents a mean discharge value lower than  $10000\text{ m}^3/\text{s}$ . The rivers presenting mean discharge values greater than  $10000\text{ m}^3/\text{s}$  represent less than 10% of the examples; here, they are kind of outliers. Then, for two reasons, we have divided the river sets in two distinguished classes:  $Q$ -Lset and its complement  $Q$ -Vset-out.

Firstly, because one expect to obtain a better ANN model if its training class is the same as those of the river test eg. an ANN trained on  $Q$ -Lset employed as a predictor for a river belonging to  $Q$ -Vset-in. Secondly, to evaluate the extrapolation capabilities (or not) of the ANN for rivers outside of the training class i.e.  $Q$ -Vset-out.

215 The numerical results presented in next section will illustrate the capabilities of the ANN for these different cases.

Note that classifying rivers within rough classes in terms of mean discharge value is realistic, for instance from the GRDC database or the GRADES database, see Lin et al. (2019).

## 3 Data-driven estimations of $Q$ by ANN

220 In this section, purely data-driven estimations of discharge are performed and analyzed. The estimations are obtained by training an Artificial Neural Networks (ANN) on the learning set  $Q$ -Lset.

### 3.1 The ANN description

The employed ANN is designed as follows. The training dataset  $\mathcal{D}$  contains  $N_{lp}$  learning pairs (“examples”)  $(I_i, Q_i)$ ,  $i = 1, \dots, N_{lp}$ . The  $i$ -th input is  $I_i = (dA, W, S, \mathcal{A})_i$  where  $i$  denotes the  $i$ -th value at the considered location and day. Recall that  $dA$  ( $\text{m}^2$ ) denotes the variations of the wetted cross-sections above the unobserved value  $A_0$ ; it is straightforwardly computed from the variations of  $Z$  ( $\text{m}$ ) and  $W$  ( $\text{m}$ ). The slopes values  $S$  are extracted from the Pepsi databases (model outputs) at SwReachSc. Values of  $\mathcal{A}$  ( $\text{km}^2$ ) are extracted from HydroSHEDS database.

Measurements are daily sampled. This frequency corresponds to the important Cal-Val phase of the forthcoming SWOT instrument. However, note that the data could be less frequent (provided eg. every few days) without altering the ANN accuracy; this point is discussed at the end of the section.

The  $i$ -th output is the discharge value  $Q_i$  at the same location and same instant (day).

The parameters of the neural network are denoted by  $W_k, k = 1, \dots, N_{hl}$ ;  $N_{hl}$  being the number of hidden layers. Each layer contains  $N_{nn}$  neurons. Since neurons are connected to each other, the size of each parameter  $W_k$  equals  $N_{nn} \times N_{nn}$ . The input variables are re-scaled by removing the mean and scaling to unit variance.

Numerous numerical experiments based on numerous different network architectures have been tested. We have observed that fairly deep networks improve the estimation capabilities (ability to find quite correctly nonlinear trends between data); From our experiments, the set  $N_{hl} = 64$  and  $N_{nn} = 64$  has proven the best precision w.r.t. performance.

Therefore  $W_1$  contains  $4 \times N_{nn} = 256$  parameters, each  $W_j, j = 2, \dots, (N_{hl} - 1)$ , contains  $N_{nn}^2 = 4096$  parameters, while  $W_{N_{hl}}$  contains  $N_{nn} \times 1 = 64$  parameters.

Training an ANN consists to solve the following optimization problem:

$$W^* = \arg \min_W l_Q(W) \quad (1)$$

with the loss function (misfit-cost function)  $l_Q$  classically set as

$$l_Q(W) = \frac{1}{N_{ls}} \sum_{i=1}^{N_{ls}} (Q_i(W) - Q^{obs}(I_i))^2 = \|Q(W) - Q^{obs}(I)\|_{2, N_{ls}}^2 \quad (2)$$

(We may also denote:  $Q_i^{obs} = Q^{obs}(I_i)$ ). The resulting estimator is:

$$Q^{(ANN)} = Q(W^*; I) \quad (3)$$

The activation function of the ANN is the usual rectified linear unit (ReLU) function, see e.g. Glorot et al. (2011); LeCun et al. (2015) for details. The ANN have been coded in Python using Keras and Mpi4Py libraries Dalcín et al. (2005). The minimization of  $l_Q(W)$  is performed using the classical Adam method Kingma and Ba (2014), a first-order gradient-based stochastic optimization. The learning rate (the gradient descent step size) is classically adjusted during the optimization procedure. As usual, the hyper-parameters of the algorithm (learning rate, decay rate, dropout probability) are experimentally chosen; the selected values are those providing the minimal value of  $l_Q$ . The reader may refer e.g. to Kanevski et al. (2009) for more details and know-hows on ANN algorithms.

*Remark.* The drainage area  $\mathcal{A}$  ( $km^2$ ) is not represented in the hydrodynamic models, at least neither (5) nor (B1). However this information is connected to the un-modeled infiltration fluxes. In other words, the ANN apparently find correlations be-

Criteria	nRMSE	NSE	$R^2$
Mean value for the 20 rivers	12.85 %	0.95	0.98

**Table 1.** Accuracy of the trained ANN for the 20 rivers of  $Q$ -Lset: obtained mean value of criteria. (Recall that these preliminary estimations are next improved by the algebraic flow model).

tween the WS measurements, the discharge and the infiltration fluxes through the drainage area value only.

### Performance criteria

260 Few criteria are used to measure the estimation accuracy: the normalized RMSE ( $nRMSE$ ), the Nash–Sutcliffe Efficiency coefficient ( $NSE$ ) and the Pearson correlation coefficient ( $R^2$ ). Applied to the variable  $Q$ , these criteria read:

-  $nRMSE(Q) = RMSE(Q) / \bar{Q}^{obs}$  with  $RMSE(Q) = (\frac{1}{n} \sum_{i=1}^n (Q_i^{est} - Q_i^{obs})^2)^{1/2}$ ,  $Q_i^{est}$  (resp.  $Q_i^{obs}$ ) is the estimated (resp. observed)  $i$ -th discharge value.

-  $NSE$  criteria reads:  $NSE = 1 - \frac{\sum_{i=1}^n (Q_i^{est} - \bar{Q}^{obs})^2}{\sum_{i=1}^n (Q_i^{obs} - \bar{Q}^{obs})^2}$ .  $NSE$  value range within  $[-\infty, 1]$ .

265 -  $R^2$  criteria reads:  $R^2(Q) = \frac{\sum_{i=1}^n (Q_i^{est} - \bar{Q}^{est})(Q_i^{obs} - \bar{Q}^{obs})}{(\sum_{i=1}^n (Q_i^{est} - \bar{Q}^{est})^2)^{1/2} (\sum_{i=1}^n (Q_i^{obs} - \bar{Q}^{obs})^2)^{1/2}}$ .

### Convergence and estimations for learned river portions

After optimization (learning stage), the loss function value (2) is low: the mean values of the misfit equals 189 ( $m^3/s$ ). The mean  $nRMSE$  and  $R^2$  over the 20 learned rivers are excellent, see Tab. 1. As a consequence the trained ANN is an excellent estimator for learned rivers. The estimated discharges for the 4 first rivers in alphabetical order are presented in Fig. 4.

270 Let us recall that uncertainty error on discharge measurements may be considered as  $\approx 30\%$  (see e.g. Gore and Banning (2017) and references therein) that is higher than the obtained nRMSE on the estimations (Tab. 1).

### 3.2 Estimations for river portions within the learning partition

Below are presented the results obtained for the 4 river portions belonging to  $Q$ -Vset-in, that is rivers not belonging to the learning set  $Q$ -Lset but presenting mean discharge values lower than 10 000  $m^3/s$ . These results are sort of K-fold cross-  
275 validations but applied to these 4 river portions only. These 4 river portions have been randomly chosen. The trained ANN is globally an excellent estimator for non-learned rivers belonging to the learning partition, see Tab. 2 and the hydrographs presented in Fig. 5. Garonne downstream, Missouri mid-section and Ohio hydrographs are very well estimated; the nRMSE are lower than 30%. Only the local peaks are not well captured. Note that in the Ohio case, the peak values are greater than 10000 ( $m^3/s$ ), that is outside the learning range. For the Iowa, the estimated hydrograph is also accurate, excepted for  
280 the lowest values. The Iowa low flows present very low discharges which are not well estimated by the ANN; therefore the relatively high nRMSE, Tab.2. In conclusion, the present simple ANN enables to accurately estimate discharge values for rivers belonging to the learning partition.

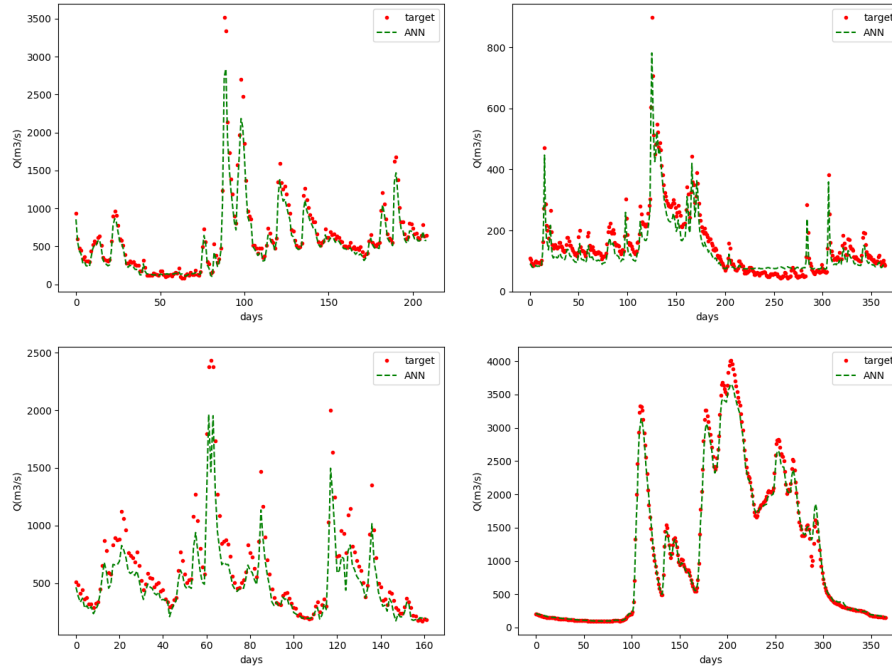


**Figure 4.** Discharge values estimated by the trained ANN for the 4 first rivers in alphabetical order belonging to  $Q$ -Lset. (Top Left) Connecticut. (Top Right) Garonne upstream. (Bottom Left) Kanawha. (Bottom Right) Kushiyara.

Rivers	nRMSE	NSE
Garonne downstream	26.6 %	0.81
Iowa	44.4 %	0.85
Missouri mid-section	18.7 %	0.85
Ohio	18.9 %	0.94

**Table 2.** Accuracy of the trained ANN for the 4 rivers of  $Q$ -Vset-in. (Recall that these preliminary estimations are next improved by the algebraic flow model)

### 3.3 Estimations for river portions outside the learning partition

Below are presented the results obtained for the 3 river portions belonging to  $Q$ -Vset-out that is presenting a great majority of discharge values greater than  $10\,000\text{ m}^3/\text{s}$ , see Fig. 2 (Top Left). The performance criteria are indicated in Tab. 3; the hydrographs are presented in Fig. 6.

As one could expect, the estimated values are greatly lower than the target ones. Rough variations of the hydrographs are partly recovered, although the peaks are greatly smoothed. Note that the target discharge values are up to 10 times the discharge values considered for the learning stage. In conclusion, as expected, a purely ANN estimation does not provide accurate estimation

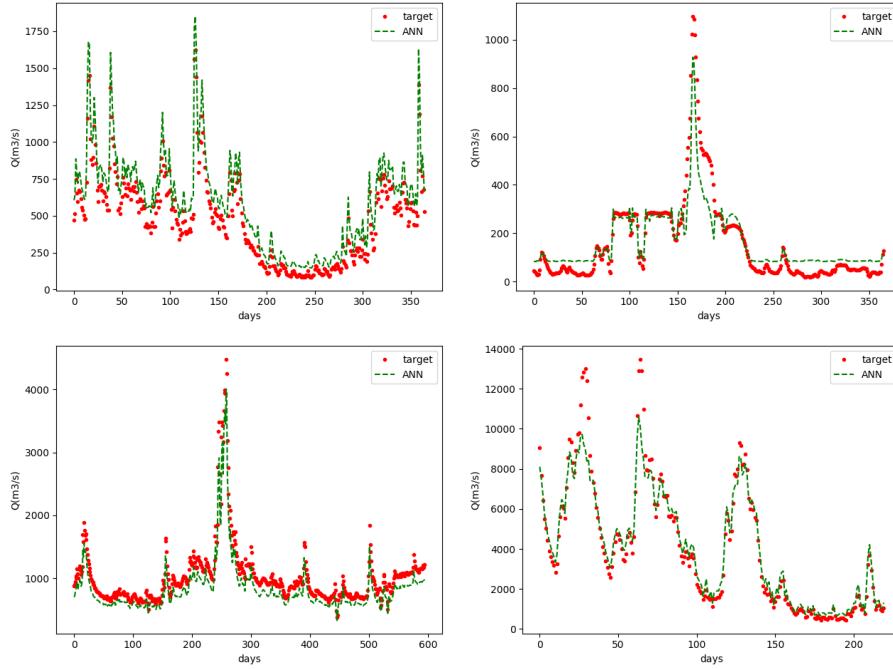


**Figure 5.** Discharge values estimated by the trained ANN for the river portions belonging to  $Q$ -Vset-in. (Top Left) Garonne Downstream. (Top Right) Iowa. (Bottom Left) Missouri mid-section. (Bottom Right) Ohio.

Rivers	nRMSE	NSE
Jamuna	73.3 %	0.28
Mississippi downstream	43.6 %	-0.56
Padma	109.4 %	-0.67

**Table 3.** Accuracy of the trained ANN for the 3 rivers of  $Q$ -Vset-out. (Recall that these first purely data-driven estimations are next improved by the algebraic flow model).

290 for rivers outside the learning partition. In other words, the ANN makes an excellent (and often an amazing) interpolator but as expected not an accurate extrapolator. However, these first ANN estimations will be employed in the sequel as a prior.

Finally let us recall that one should generally be able to classify rivers by rough classes in terms of mean discharge from eg. the GRADES database, Lin et al. (2019). As a consequence, for a majority of rivers portions, one should be able to perform the ANN estimation within the learning partition and not outside, like it is done here.

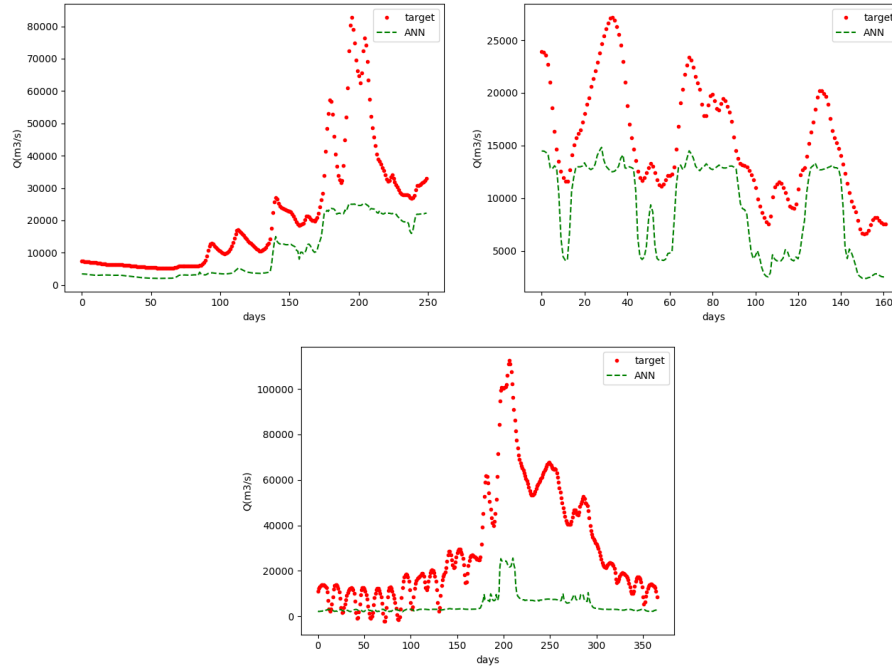


**Figure 6.** Discharge values estimated by the trained ANN for river portions belonging to  $Q$ -Vset-out that is rivers presenting discharge values outside the learning partition. (Top Left) Jamuna. (Top Right) Mississippi downstream. (Bottom) Padma.

### 295 3.4 On the sensitivity of the estimations with respect to error measurements and data frequency

As already mentioned, as a first step and following the Pepsi 1 and Pepsi 2 Durand et al. (2016); Frasson et al. (Submitted) benchmarks design (from the Discharge Algorithm Working Group of the SWOT Science Team), algorithms evaluations are performed on data with no noise and 1 day sampling. Recall that the first SWOT observations will have a 1 day repeat period during the Cal/Val phase. The next phase of algorithms evaluations consists to introduce realistic noise and time sampling.

300 Finally the last phase consists to consider outputs from the SWOT Science Simulator or data from AirSWOT (AirBorne) campaigns. This gradual approach is scientifically necessary to demonstrate the estimations capabilities of the methods, their robustness and their weakness or inaccuracy origins. This is the approach we rigorously follow here to evaluate the present new method capabilities.

305 However, we have performed numerous tests to be confident in the method robustness, its relative insensitivity with respect to a few data properties. First, we have performed numerous ANN estimations with different test and train sets; demonstrating the robustness (and its relative accuracy) of the purely data-driven estimations. Second, we have tested the sensitivity of the present ANN estimations with respect to : a) the noise on the WS measurements ( $Z, W$ ) ; b) the data frequency. The results

analysis are presented below.

310

*With noisy WS measurements ( $Z, W$ ).* We have tested the ANN estimation if considering perturbed measurements ( $Z, W$ ), respecting the expected instrument accuracy. Data have been perturbed by Gaussian noises with  $\sigma_Z = 0.25\text{m}$  (resp.  $\sigma_W = 5.0\text{m}$ ) for  $Z$  (resp.  $W$ ) for 1-day repeat. The obtained results are as follows: NRMSE equals 18.1% and NSE equals 0.91. These results have to be compared with those indicated in Table 1, that is: 18.1% vs 12.8% and 0.91 vs 0.98. These results show that the ANN estimations remain robust to the inaccuracy of the WS measurements.

*With less frequent WS measurements.* In the present ANN, the concept of spatial correlation or time correlation between the examples does not exist. Indeed, each "example" corresponds to a set of  $(4 + 1)$  values which are correlated neither in time nor in space; they are simple point-wise snapshots. As a consequence, the ANN does not "see" any space or time structure in the datasets. After optimization (training), an optimal ANN model has been built. The latter enables to reproduce invariants between the four input variables and the output variable  $Q$ . This is a classical amazing feature of ANNs, see eg. Mallat (2016), despite no one fully understand how it actually works yet. The ANN validation consists to test on numerous aleatory train - test datasets. This is what it has classically been done here.

325 Following the argument above, the present ANN has to provide a similar accuracy if considering much less frequent observations, but with the same volume and same quality of data of course. We have investigated this assertion for a frequency of 5 days. As expected the obtained accuracy were similar to those presented in Table 2. Note that the performances of ANN experiments are never exactly the same since based on aleatory features. Obviously, in this case, the discharge estimations remain valid for a few hours - a day around the observation instant only. Indeed let us recall that the time validity of the discharge estimation is approximatively equal to the wave travelling time through the river portion (roughly, a few hours to a day), see eg. Paiva et al. (2015); Brisset et al. (2018); Larnier et al. (2020a) for such a discussion.

335 Let us recall that if considering the nominal SWOT orbit (21 days repeat orbit) with noisy data, the scientific challenge which consists to solve the inverse problem for ungaged rivers remains of same nature as the present one; of course with higher uncertainties and a time limitation of the discharge estimations (which equal the wave travelling time through the river portion).

#### 4 Physically-based estimations using the algebraic flow model: first guesses

In this section, the low Froude flow model is presented; it is an algebraic system. The Strickler friction coefficient  $K$  has to depend on space and time, then to reduce its complexity, it is modeled as a power-law in water depth  $h$ . Next given the WS

340

measurements and  $Q^{(ANN)}$ , the algebraic flow model is solved to obtain estimations of  $(A_{0,r}, (\alpha, \beta)_r)$  and  $Q_{in,p} \forall r, p$ . These estimations will be next considered as the first guess values in the VDA based inversion presented in next section.

#### 4.1 Reduced parametrization of $K$

Following Garambois et al. (2020); Larnier et al. (2020a), the Strickler friction coefficient  $K$  is defined as local power-laws at  
 345 SwReachSc:  $K_{r,p} \equiv K((\alpha_r, \beta_r); h_{r,p}) = \alpha_r (h_{r,p})^{\beta_r} \quad \forall r \forall p$ . As a consequence, given  $R \times (P+1)$  measurements  $Z_{r,p}$ , the friction parameter  $K_{r,p}$  is represented by  $2R$  parameters only:  $(\alpha_r, \beta_r)_{1 \leq r \leq R}$ . This reduced parametrization provides a local effective power-law in  $h$ . The law reads in function of the WS measurements as:

$$K_{r,p} \equiv K((\alpha_r, \beta_r); A_{0,r}, W_{r,0}, Z_{r,p}) = \alpha_r \left( Z_{r,p} - Z_{r,0} + \frac{1}{W_{r,0}} A_{0,r} \right)^{\beta_r} \quad \forall r \forall p \quad (4)$$

350

In the sequel if one refers to the friction parameter  $K_{r,p}$ , this actually refers to its parametrization defined by (4).

#### 4.2 The algebraic flow model

While deriving the flow equations (mass and momentum conservation laws), the Low Froude assumption ( $Fr^2 \ll 1$ ) is applied. The resulting model is an algebraic system of  $R$  equations (one equation per reach  $r$ ); each equation is similar to the  
 355 Manning-Strickler law, see Larnier et al. (2020a); Brisset et al. (2018). Since this “Low Froude” flow model is algebraic, its complexity is low. Using the present reduced parametrization (4), this system reads as follows:

$$Q_{r,p}^{\frac{3}{5}} = \alpha_r^{3/5} (c_{r,p}^{(1)} A_{0,r} + c_{r,p}^{(2)}) \left( c_r^{(4)} A_{0,r} + c_{r,p}^{(3)} \right)^{3/5 \beta_r} \quad 1 \leq r \leq R, \quad 0 \leq p \leq P \quad (5)$$

The coefficients  $c_{r,p}^{(k)}$ ,  $k = 1, \dots, 3$ , and  $c_r^{(4)}$  can be evaluated from the altimetry measurements. Their expressions are:

$$c_{r,p}^{(1)} = W_{r,p}^{-\frac{2}{5}} S_{r,p}^{3/10}, \quad c_{r,p}^{(2)} = c_{r,p}^{(1)} \delta A_{r,p}, \quad c_{r,p}^{(3)} = (Z_{r,p} - Z_{r,0}), \quad c_r^{(4)} = \frac{1}{W_{r,0}} \quad (6)$$

360 System (5) constitutes the so-called algebraic flow model. It contains  $R(P+1)$  equations.

If considering the full set of unknowns  $((\alpha_r, \beta_r), A_{0,r}, Q_{r,p})$  i.e.  $R(3 + (P+1))$  unknowns, it is an underdetermined system therefore admitting an infinity of solutions.

If the discharge values  $Q_{r,p}$  are given, the system admits a unique solution for the two other variables  $((\alpha_r, \beta_r), A_{0,r})$  ( $2R$  unknowns). This is the way the first guesses  $(K_{r,p}, A_{0,r})^{(0)}$  are computed given  $Q_{r,p}^{ANN}$ , see Section 4.3.

365 Moreover this system will be employed differently to compute real-time estimations of  $Q$ , see Section 7.

Finally it is worth to notice that if  $A_{0,r}$  is given  $\forall r$  (therefore all wetted areas  $A_{r,p} = A_{r,0} + \delta A_{r,p} \forall r \forall p$  are given) then by solving the algebraic flow model (5) the inference of the *ratio*  $(Q/K)_{r,p}$  is possible but not the sought variables  $(Q_{r,p}, K_{r,p})$ . (Of course, this remark applies to the classical scalar Manning-Strickler’s law too).

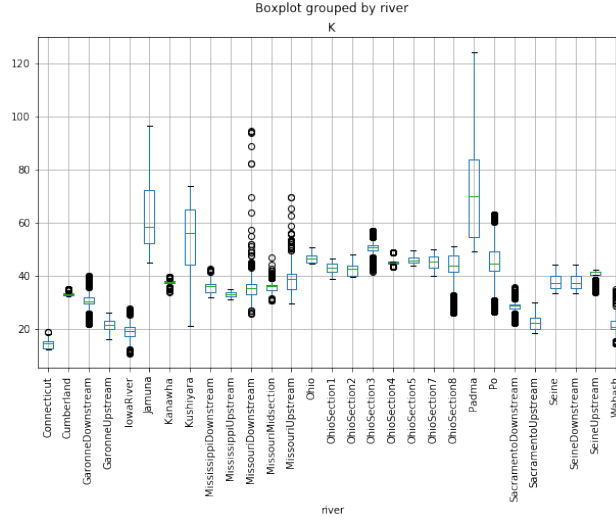


**Figure 7.** Effective Strickler friction coefficient  $K$  computed by solving the low Froude (algebraic) flow model (5), given data of the considered river portions.

### Effective low Froude flow Strickler values

370 Given the datasets presented in Section 2.2, the friction coefficient  $K$  corresponding to the low Froude flow model is computed by solving (5), see Fig. 7. This is an effective low Froude Strickler coefficient. This plot highlights the large range value of the effective low Froude Strickler coefficient; also it confirms physically-consistent values of  $K$  obtained from the other measurements.

### 4.3 First guesses $(A_{0,r}, (\alpha, \beta)_r)^{(0)}$ and $Q_{in,p}^{(0)}$

375 In next section the VDA formulation is presented. It aims at estimating the unknown “input parameters” of the Saint-Venant flow model which are: the time-dependent discharge at inflow  $Q_{in}(t)$ , the bathymetry  $b(x)$  (equivalent to  $A_0(x)$ ) and the friction coefficient  $K$  (parametrized as  $K(h(x, t))$ , see (4)). The VDA algorithm is iterative; the choice of a good first guess is important. Below is presented how the first guess values  $(A_{0,r}, (\alpha, \beta)_r)^{(0)}$  and  $Q_{in,p}^{(0)}$  are computed.

#### 4.3.1 First guess $(A_{0,r}, (\alpha, \beta)_r)^{(0)}$

380 Given the WS measurements and  $Q^{(ANN)}$  (the discharge estimation obtained by ANN, see (3)), values of  $(A_0(x), K)$  are estimated by solving the algebraic flow model (5). These values provide the first guesses values  $(A_0^{(0)}(x), K^{(0)}(h(x, t)))$  in the VDA algorithm. Recall that the Strickler friction coefficient  $K$  is space-time dependent through the reduced parametrization (4). Given  $Q_{r,p}^{ANN}$  (discharge estimation for reach  $r$  at instant  $p$ ), the algebraic system is solved by using the Metropolis-Hasting algorithm (MCMC method) to obtain  $(A_{0,r}, (\alpha_r, \beta_r))^{(0)}$ .

385 In the Metropolis-Hasting algorithm, the a-priori pdf are as follows:  $\mathcal{U}(10, 100)$  for  $\alpha_r$ ,  $\mathcal{N}(0, 0.3)$  for  $\beta_r$  and  $\mathcal{N}(\mu_{A_0/\bar{A}}, \sigma_{A_0/\bar{A}})$  for  $(A_0/\bar{A})_r$ . Following the statistics obtained from the HydroSWOT and Pepsi databases  $\mu_{A_0/\bar{A}} = 0.73$ ,  $\sigma_{A_0/\bar{A}} = 0.21$ .

Given  $A_{0,r}^{(0)}$  and the measurements  $(Z_{r,0}, W_{r,0})$ , the corresponding bathymetry profile  $b_r^{(0)}$  is explicitly obtained, see Section 2.1. These bathymetry values are the “prior” plotted in figures 13 and 12.

390 The target bathymetry values are those employed in the various calibrated reference flow models (HEC-Ras, LisFlood etc) which have been performed to obtain the synthetic data available in the Pepsi 1 and Pepsi 2 datasets, see Durand et al. (2016); Frasson et al. (Submitted) and references therein. In the figures 11, 12 and 13, the “true” (target) values are represented by the red dots. The latter are computed from the effective rectangular values of the unobserved lowest cross-section  $A_0$  ( $W = W_0, H_0 = Z_0 - b$ ). These “true” values of bathymetry  $b$  and  $A_0$  are available at Reference Data Scale only (see Section 2).

395

### 4.3.2 First guess $Q_{in,p}^{(0)}$

Given  $(A_{0,r}, (\alpha_r, \beta_r))^{(0)}$ , the first guess  $Q_{in,p}^{(0)}$  is explicitly obtained from the algebraic flow model (5). First guess values  $Q_{in,p}^{(0)}$  are plotted in Fig. 13 (“prior” curve) for rivers within the learning partition and in Fig. 12 (“prior” curve) for rivers outside the learning partition. In both cases, these low Froude estimations  $Q_{in,p}^{(0)}$  better catch the variations of the true values than  $Q^{(ANN)}$  (indicated as “ANN” on the figures). The estimation  $Q_{in,p}^{(0)}$  may be viewed as a physically-consistent correction of the purely data driven estimation  $Q^{(ANN)}$ . *Remark.* If a mean value of  $Q^{(true)}$  is known for a given period (e.g. a week, a month), then one can make fit this information with  $Q_{in,p}^{(0)}$ . Then, with such an information  $Q_{in,p}^{(0)}$  would already be an excellent estimation. However in ungauged rivers, such mean value is unavailable.

## 405 5 Physically-based estimations of $(Q(x, t), A_0(x), K(x; h(x, t)))$ by Variational Data Assimilation (VDA)

VDA aims at estimating the unknown “input parameters” of the Saint-Venant flow model which are the time-dependent discharge at inflow  $Q_{in}(t)$ , the bathymetry  $b(x)$  (equivalently  $A_0(x)$ ) and the friction coefficient  $K$  ( $K$  is parametrized as indicated in (4)). The data (WS measurements) are employed as follows. The elevation values  $Z$  are used in the cost function which measures the misfit, see (8),  $W$  is used to build up the efficient cross-sections geometry of the Saint-Venant flow model, 410 see Section A, while the slope values  $S$  are used in the algebraic flow model only, see (5).

### 5.1 The VDA formulation

The employed VDA formulation is the one developed in Larnier et al. (2020a) with a few improvements. At the observation scale, the discrete unknown “parameters” of the dynamic flow model (Saint-Venant’s equations) reads:

$$c = (Q_{in,0}, \dots, Q_{in,P}; b_1, \dots, b_R; (\alpha_1, \beta_1), \dots, (\alpha_R, \beta_R))^T \quad (7)$$

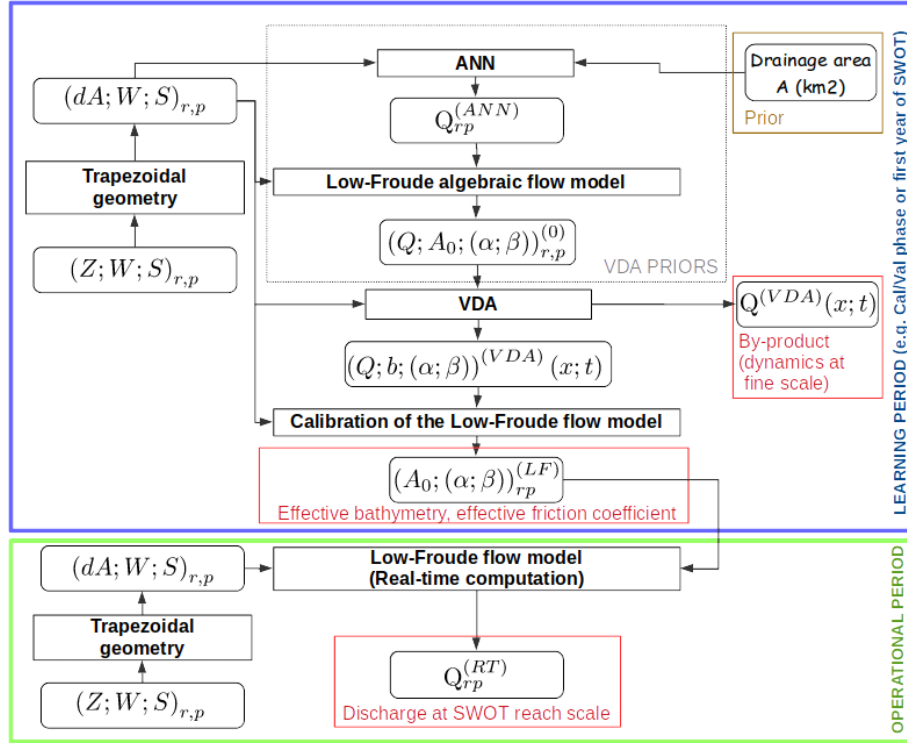


**Figure 8.** FlowChart of the complete inversion algorithm. Input data are the WS measurements  $(Z, W, S)$  at SwReachSc (SWOT like). Prior is  $\mathcal{A} (km^2)$  only (from eg. HydroSHEDS database). After the learning period (eg. one year), effective bathymetry  $b(x)$  (equivalently  $A_0(x)$ ) and low-Froude effective friction coefficients  $K(x; h)$  are estimated (plus discharge values at the fine CompGridSc scale). Next, during the operational period, given newly acquired WS measurements, discharges are computed in real CPU-time at SwReachSc.

415 The subscript  $p$  denotes the instant,  $p \in [0..P]$ ,  $r$  denotes the reach number,  $r \in [1..R]$ , see Fig. A1. The parameters used to impose a normal depth at downstream, see Section B, are considered as unknown parameters too (otherwise the flow would be controlled by the imposed outflow condition).

The cost function aims at measuring the misfit between data (therefore at the observations scale) and the Saint-Venant (fine scale) flow model output. It is defined as:

$$420 \quad j(c) \equiv j_{obs}(c) = \frac{1}{2} \sum_{p=0}^P \sum_{r=1}^R (Z_{r,p}(c) - Z_{r,p}^{obs})^2 \quad (8)$$

This cost function  $j$  has to be minimized, starting from a first guess value (prior)  $c^{(0)}$ . However following Lorenc et al. (2000); Larnier et al. (2020a), the following change of variable is applied:

$$k = B^{-1/2}(c - c^{prior}) \quad (9)$$

with  $B$  a covariance (symmetric definite positive) matrix,  $B = B^{1/2}B^{1/2}$ .

425 Then by setting  $J(k) = j(c)$ , the considered optimization problem reads:

$$\min_k J(k) \tag{10}$$

The first order optimality condition of this optimization problem reads:  $B^{1/2}\nabla j(c) = 0$ . The change of variable based on the covariance matrix  $B$  acts as a preconditionner for the optimization problem, see e.g. Haben et al. (2011a, b) for related analysis.

Recall that in the linear-quadratic case (the model is linear, the functional is quadratic), one can show the equivalence  
 430 between the VDA solution of (10) (considering (9)) and Bayesian estimations based on  $B$ , see e.g. Monnier (2020). The VDA algorithm is implemented in the DassFlow computational code Larnier et al. (2020b); it employs the automatic differentiation tool Tapenade Hascoët and Pascual (2013).

It is necessary to add a regularization (“convexifying”) term to the cost function  $j(c)$  to define a better conditioned optimization problem, see e.g. Bouttier and Courtier (2002). The classical way to do it is to define  $j$  as follows:  $j(c) = j_{obs}(c) + j_{reg}(c)$   
 435 with  $j_{reg}$  a Tikhonov regularization term. Here the regularization term reads as:

$$j_{reg}(c) = \frac{1}{2} \left( \gamma_b \sum_{r=1}^R |\partial_r b_r(c)|^2 + \gamma_\alpha \sum_{r=1}^R |\partial_r \alpha_r(c)|^2 \right).$$

The regularization term weight coefficients  $\gamma_\square$  are empirically set (making at the initial iteration the regularization terms  $\approx 10\%$  of  $j_{obs}$ ). Following an adaptive regularization strategy, see e.g. Kaltenbacher et al. (2008), the weight coefficients are divided by 2 every 10 iterations.

440 Moreover thanks to the formulation (9), a regularization term is also implicitly introduced through the covariance matrix  $B$  too. Indeed one can show the equivalence between the chosen covariance kernel  $B$  (e.g. as the second order auto-regressive kernel like those employed below, see (12)) and a regularization functional. The reader may refer to e.g. Tarantola (2005); Monnier and Zhu (2019) for detailed examples. The definition of  $B$  is detailed in the next subsection.

445 *Remark.* Compared to the HiVDI algorithm presented in Larnier et al. (2020a) (and implemented in Larnier et al. (2020b)), a technical but important improvement have been introduced. The vertical discretization of the river geometry (superimposition of the measured trapeziums, see Section A) is now represented by a smooth curve parametrized by a very low number of points (eg. 5); these points being optimal in the sense they minimize the  $R^2$  (Pierson) criteria. Defining a regularized vertical geometry is important since it is differentiated in the reverse code. Indeed the adjoint method (implemented using automatic differentia-  
 450 tion) computes the differential of the geometry function. Therefore if this function presents numerous stiff local gradients, this may affect the algorithm convergence robustness. The present regularized geometry provides more robust convergence of the optimizer while it remains physically-consistent.

## 5.2 Setting the covariance matrix $B$

455 The choice of  $B$  greatly determines the computed solution of the inverse problem; this “prior model  $B$ ” constitutes an important feature of the VDA formulation. In the present study, these covariances are defined from classical operators but with non constant coefficients therefore defining somehow physically-adaptive regularizations.

### 5.2.1 Expression of $B$

Here the three unknown parameters  $(Q_{in}(t), b(x), K(x))$  are supposed to be independent variables. This assumption is a-priori  
460 incorrect but one don’t know a-priori universal covariances between these variables. As a consequence  $B$  is defined as a block diagonal matrix:

$$B = \text{blockdiag}(B_{Q_{in}}, B_b, B_K) \quad (11)$$

Each block matrix  $B_{\square}$  is defined as a covariance matrix (symmetric positive definite matrix). The matrices  $B_Q$  and  $B_b$  are set as the classical second order auto-regressive correlation matrices:

$$465 \quad (B_{Q_{in}})_{i,j} = (\sigma_{Q_{in}}(t))^2 \exp\left(-\frac{|t_j - t_i|}{T_{Q_{in}}}\right) \text{ and } (B_b)_{i,j} = (\sigma_b(x))^2 \exp\left(-\frac{|x_j - x_i|}{L_b}\right) \quad (12)$$

The matrix  $B_K$  is set as  $B_K = \text{blockdiag}(B_{\alpha}, B_{\beta})$  with:

$$(B_{\alpha})_{i,j} = \sigma_{\alpha}^2(x) \exp\left(-\frac{|x_j - x_i|}{L_K}\right) \text{ and } B_{\beta} = \text{diag}(\sigma_{\beta}^2(x)) \quad (13)$$

The parameters  $T_{Q_{in}}$  and  $(L_b, L_K)$  act as correlation lengths.

### 5.2.2 Setting of the parameters $\sigma_{\square}$ and $(T_{Q_{in}}, L_{\square})$

470 These parameters are important prior information of the inversions. They are set from the first guesses values  $(Q_{in,p}, A_{0,r}, (\alpha, \beta)_r)^{(0)}$ .

Recall that the observation frequency is 24h. The measurements spacing varies from a few dozen meters to a few hundreds of meters. Local Froude numbers range in great majority within  $\approx [0.05 - 0.3]$ , with some very local maximum values up to  $\approx 0.5$ .

The discharge parameters are set as follows.  $T_{Q_{in}} = 24$  h. The normalization coefficient  $\sigma_{Q_{in}}$  is time-dependent:  $\sigma_{Q_{in}}(t)$   
475 equals 30% of the mean value of  $Q^{(0)}(t)$ . (Recall that uncertainty error on discharge measurements may be considered as  $\approx 30\%$ , see e.g. Gore and Banning (2017) and references therein).

Concerning the bathymetry,  $\sigma_b$  is space dependent:  $\sigma_b(x)$  is set such that it corresponds to  $P_{\sigma_b} = 50\%$  of the mean value of  $A_0^{(0)}(x)$ . Recall that the bathymetry values  $b^{(0)}(x)$  are deduced from the unobserved flow area values  $A_0^{(0)}(x)$ .

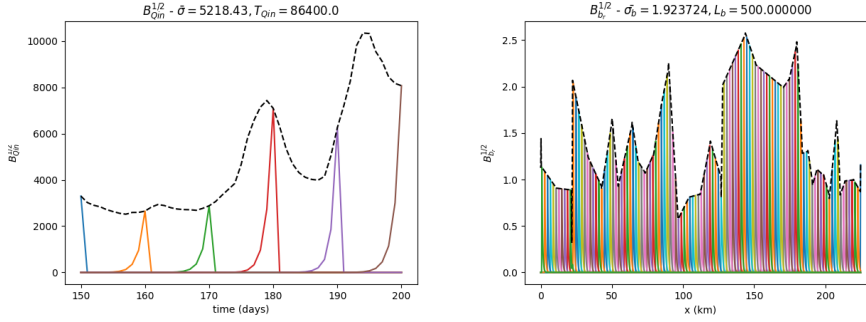


**Figure 9.** The covariance matrices  $B_{\square}^{1/2}$  in the Jamuna river case. (L)  $B_{Q_{in}}^{1/2}$  (with  $T_{Q_{in}} = 24h$ ). A few covariance values only are plotted for sake of readability. (R)  $B_b^{1/2}$  (with  $L_b = 500m$ ). Note that the scaling factor of  $B_{\square}^{-1/2}$  is  $\sigma_{\square}^{-1/2}$  and not  $\sigma_{\square}$ .

Concerning the correlation length, we set:  $L_b = 1$  km. However if this last parameter is too large, the matrix  $B_b$  may be not  
 480 positive. In such a case, the characteristic length  $L_b$  is adaptively decrease until the matrix becomes positive. This has happened  
 in a few cases, then the minimal resulting value was  $L_b = 500$  m.

The normalization coefficients related to the friction are constant:  $\sigma_{\alpha} = 10$  and  $\sigma_{\beta} = 0.3$ . These values have been chosen  
 following statistical analysis made on the databases and by analyzes on the gradient components. We set  $L_{\alpha} = dx = 100m$  ( $dx$   
 is the computation grid spacing).

485 As an illustration, some covariance matrices  $B_{\square}$  are plotted in Fig. 9.

### 5.3 Capabilities and limitations of the inversions based on the flow models only

The (low-complexity) algebraic flow model (based on the Low-Froude assumption  $Fr^2 \ll 1$ , see Garambois and Monnier  
 490 (2015); Brisset et al. (2018)), enables to determine the ratio  $Q/\alpha$ , equivalently  $Q/K$ , and not the unknowns pair  $(Q, K)$ . This  
 remarks holds even if the bathymetry  $b$  (equivalently  $A_0$ ) is known.

This remarks also holds of course for the usual scalar Manning-Strickler's equation.

Let us show that the inverse problem aiming at estimating the triplet  $(Q_{in}(t), A_0(x), K(h(x, t)))$  in the Saint-Venant system  
 495 (B1) is also ill-posed in the following sense: the model solution  $(A, Q)(x, t)$  is unchanged by multiplying these unknown  
 parameters by an adequate multiplicative factor.

Let  $\bar{Q}$  be any scalar value:  $\bar{Q}$  may be a mean value of  $Q$  or  $K$ . Let us define the following re-scaled state variables:  $(A_*, Q_*) =$   
 $(A, Q)/\bar{Q}$ . The mass equation (B1)(a) divided by  $\bar{Q}$  is unchanged therefore:  $\partial_t(A_*) + \partial_x(Q_*) = 0$ . The mass equation still  
 holds;  $Q$  simply implies to rescale  $A$  by the same factor.

500 The re-scaled momentum equation ((B1)(b) divided by  $\bar{Q}$ ) reads:

$$\partial_t(Q_*) + \partial_x \left( \frac{Q_*^2}{A_*} \right) + gA_* \partial_x Z = -gA_* S_f \quad (14)$$

with  $S_f \equiv S_f(A, Q; h; K) = \frac{1}{K^2} \frac{|Q|Q}{A^2 h^{4/3}}$ . If defining  $h$  as the effective cross-section depth:  $h = A/W$ ,  $W$  the WS width, then:  $S_f(A, Q, h; K) = S_f(A_*, Q_*, h_*; \bar{Q}^{-2/3} K)$ .

Therefore, given the WS measurements  $(W, Z)$ , the 1D Saint-Venant equations (B1) with parameter  $K$  are equivalent to the  
 505 same equations in the re-scaled variables  $(A_*, Q_*)$  but with  $(\bar{Q}^{-2/3} K)$  as Manning-Strickler's parameter. Concerning bound-  
 ary conditions, both upstream and downstream conditions are transparently re-scaled by the factor  $\bar{Q}$ . This little calculation has  
 been first presented in Larnier et al. (2020a).

It is worth noticing that this calculation and its consequences remain of course true for the non-inertial version of the Saint-  
 Venant model classically employed in hydrodynamic river flow codes.

510

A consequence of this “equifinality issue” is the following: at each minimization iteration in the VDA process (see Section  
 5 for details), the “model constraint” (B1) is satisfied by an infinity of flow states values  $(A, Q)$  characterized by the parameter  
 $K$ . In other words, the flow model (B1) constrains the inverse problem solution  $(Q_{in}(t), A_0(x), K(h))$  up to a multiplicative  
 factor only. This property is of course observed in the numerical results (see Section 6.3): the space-time variations of discharge  
 515 are accurately inferred, however with a bias. This bias depends to the prior information introduced in the inverse method. The  
 introduced priors in the present VDA formulation are detailed in Section 5.3.

In the case the bathymetry  $b(x)$  is given (therefore  $A_0(x)$ ), the re-scaled unknown  $(A, Q^*)$  does not satisfy the flow model  
 anymore. In other words, if the bathymetry is given, the inverse problem based on the Saint-Venant model (B1) may be well  
 520 posed. Moreover it has been demonstrated in Garambois and Monnier (2015); Brisset et al. (2018) that a single measurement  
 of bathymetry (i.e. at a single location) enables an accurate estimation of the bathymetry along a relatively long river portion.

In the case, a (simple scalar) mean value of  $Q$  is known (e.g. seasonal or annual value), the bias issue is solved ! The inverse  
 problem may be well-posed. The numerical results confirm this assertion, see Section 6.3: in such a case, the estimations of  
 525  $Q(x, t)$  are accurate, without bias.

The model-constraint of the optimization problem (10) is constraining (in space-time) but up to a multiplicative factor  
 only. The VDA solution (solution of (10) under the dynamic flow model constraint) depends on the prior: the first guess but  
 also the covariance matrix  $B$ , see Section 5.2. The introduction of  $B$  is necessary to make the algorithm convergence robust.  
 530 However the solution has to satisfy this prior probabilistic model  $B$  (defined from the prior parameters  $\sigma_\square$ ). Therefore, the  
 prior parameters  $\sigma_\square$  play an important role in the determination of the optimal solution. This feature of the VDA process is

well known, see e.g. Lorenc (1988); Haben et al. (2011b) and references therein. (Also the reader may refer e.g. to Monnier (2020) for a formal proof showing the equivalence between VDA covariance based solutions and Bayesian estimations).

In the present approach, the first guesses  $(Q_{in}(t), A_0(x), K)^{(0)}$  of the minimization algorithm are consistent with the algebraic flow model (5). This model (5) defines a physically-consistent solution, however up to the multiplicative factor. Next, the descent algorithm explores the optimal solution in a “vicinity” of a physically-consistent solution, the provided first guess  $(Q_{in}(t), A_0(x), K)^{(0)}$ . In practice, and as illustrated by the numerical results shown in next sections, the space-time variations of  $Q$  are always accurately identified but the global estimation may still present a bias; the latter depending on the accuracy of the first guess value  $Q_{in}^{(0)}$  in particular.

## 540 6 Estimations obtained by VDA

In this section, numerical results based on the VDA method are presented. Given a first guess  $(Q_{in,p}^{(0)}, A_{0,r}, (\alpha, \beta)_r)^{(0)}$  computed as indicated in Section 4.3, the optimization problem (10) is solved by a minimization algorithm, see Section 5. First, typical behaviors and accuracy of the minimization algorithm are briefly presented. Next, numerical results are presented for two river portions (randomly chosen) belonging to  $Q$ -Vset-in, rivers presenting mean discharge values within the learning range (i.e. lower than  $10\,000\,m^3/s$ ) but outside the learning partition  $Q$ -Lset, see Section 2.3. Finally, numerical results are presented for two river portions (randomly chosen) belonging to  $Q$ -Vset-out, that are rivers presenting mean discharge values outside the learning range (i.e. greater than  $10\,000\,m^3/s$ ), see Section 2.3.

As indicated in Section 2, the target bathymetry values are those employed in the various calibrated reference flow models (HEC-Ras, LisFlood etc) which have been performed to obtain the synthetic data available in the Pepsi 1 and Pepsi 2 datasets, see Durand et al. (2016); Frasson et al. (Submitted) and references therein. In the figures 11, 12 and 13, these “true” (target) values are represented by the red dots. The latter are computed from the effective rectangular values of the unobserved lowest wetted cross-section  $A_0$ , with  $(W = W_0, H_0 = Z_0 - b)$ . These values of bathymetry  $b$  and  $A_0$  are available at Reference Data Scale only.

555

### 6.1 On the VDA algorithm convergence

The minimization algorithm aiming at solving (10) converge generally in less than 100 iterations; and in some complex case, the convergence may be reached after more than 150 iterations, see e.g. Fig. 10. After convergence, the misfit values on WS elevation, see (8), is always excellent: standard deviation  $\sigma_{misfit} \approx 10$  cm, see Fig. 10. This value of  $\sigma_{misfit}$  is lower than the expected value for SWOT instrument ( $\sigma_{SWOT} = 25$  cm, see Rodriguez and others (2012)).

560

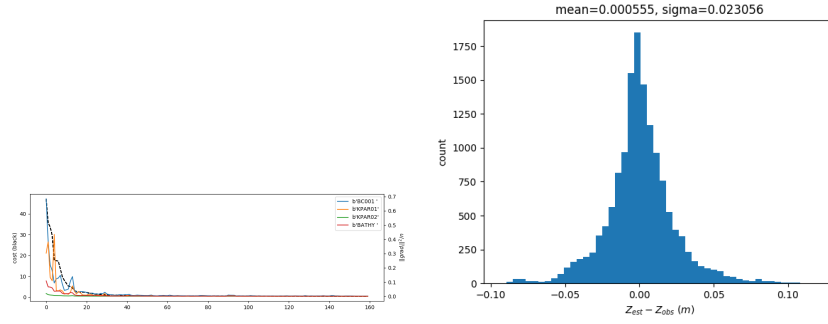


**Figure 10.** VDA algorithm convergence: (Left) A typical convergence curve: cost function  $J(k)$  (dashed black line) and gradient components (colored solid lines) vs iterations (Garonne Downstream case). 'BCOO1', 'KPAR01', 'KPAR02', 'BATHY' corresponds to the gradient component wrt to  $Q_{in}(t)$ ,  $\alpha(x)$ ,  $\beta(x)$ ,  $b(x)$  respectively (all in norms 2). (Right) Misfit values  $|Z_{r,p} - Z_{r,p}^{obs}| \forall r \forall p$  in meters (see (8)) after convergence.

## 6.2 Numerical results for rivers within the learning range but outside the learning partition $Q$ -Lset

Numerical results for Garonne downstream and Ohio river portions (randomly chosen) belonging to  $Q$ -Vset-in are presented in Fig. 5. They are rivers presenting a mean discharge value within the learning range (i.e. lower than  $10\,000\,m^3/s$ ) but outside the learning partition  $Q$ -Lset, see Section 2.3. As previously mentioned, the first guess values  $(Q_{in,p}; A_{0,r}, (\alpha, \beta)_r)^{(0)}$  are  
565 computed by solving the algebraic flow model given the WS measurements and the prior  $Q^{(ANN)}$ . Performance criteria are indicated in Tab. 4; the estimations are plotted in Fig. 11 ("prior (VDA)" denotes  $Q_{in,p}^{(0)}$ ).

The three estimations (ANN, first guess and VDA solution) are excellent. Again, the nRMSE are lower than the standard error made on discharge measurements. Again, the VDA estimation (physically-based) captures better the variations than the purely data-driven estimation (ANN).

570 Concerning the bathymetry, in the Garonne case, the VDA clearly improve its estimation, in particular in pools (low values of  $b(x)$ ), Fig. 11 (Down)(L). In the Ohio case, the bathymetry estimation remains relatively inaccurate despite the excellent discharge estimation. In such a case, the bathymetry error is balanced by a Strickler coefficient adjustment.

## 6.3 Numerical results outside the learning range

Numerical results for Jamuna and Mississippi downstream portions (randomly chosen) belonging to  $Q$ -Vset-out are presented in  
575 Fig. 12. They are rivers presenting a mean discharge value outside the learning range (i.e. greater than  $10\,000\,m^3/s$ ) therefore outside the learning partition  $Q$ -Lset too, see Section 2.3.

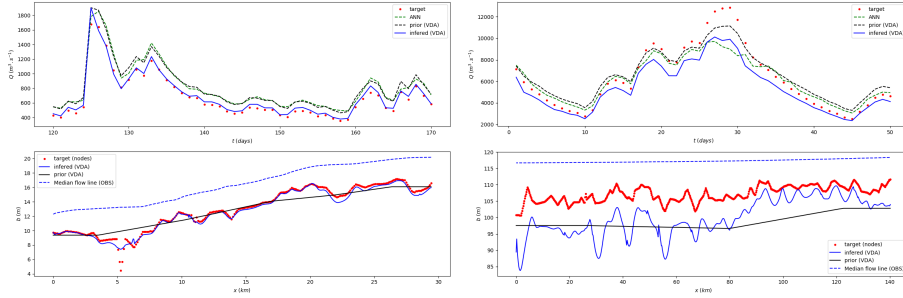


**Figure 11.** Discharge estimations for 2 rivers (randomly chosen) belonging to Q-Vset-in. (Left column) Garonne downstream. (Right column) Ohio.

(Up) Discharge values  $Q_{in}(t)$  vs time during the assimilating period only. (Down) Bathymetry values  $b(x)$  and the observed median flow line  $Z_{med}^{(obs)}(x)$ .

River name	ANN prior	nRMSE	NSE
Garonne downstream	$Q^{(ANN)}$	28.6 %	0.78
Ohio	$Q^{(ANN)}$	18.5 %	0.84
Jamuna	$Q^{(ANN)}$	71.2 %	-0.56
Mississippi downstream	$Q^{(ANN)}$	46.1 %	-1.00
Jamuna	$2Q^{(ANN)}$	39.4 %	0.52
Mississippi downstream	$2Q^{(ANN)}$	15.0 %	0.78

**Table 4.** Performance obtained on the discharge estimation  $Q^{(VDA)}$ .

### 6.3.1 Estimations from the prior $Q^{(ANN)}$

In this first experiment, the considered prior discharge value is  $Q^{(ANN)}$ , like in all previous numerical experiments. Recall that this prior is inaccurate since the rivers do not present mean discharge values within the learning range, see Section 3.3. The  
580 obtained estimations are presented in Fig. 12 (where “prior” denotes  $Q_{in,p}^{(0)}$ ); performance criteria are indicated in Tab. 4.

In the Jamuna case, the VDA estimation is better than the provided first guess, that is the algebraic flow model solution (“prior VDA” in Fig. 12). This estimation captures quite well the time discharge variations; however it remains an under-estimation of the true value. The bathymetry estimation is not a real improvement of the prior value. Note that its oscillations can be easily smoothed by increasing the weight of the regularization term, see Section 5.1.

585 In the Mississippi case, the VDA estimation captures well the discharge variations, better than ANN again, but it deteriorates the global accuracy. In this case, the prior introduced in the covariance matrix  $B$  are not satisfying. These two examples illustrate the phenomena previously mentioned: a) the flow models act as physically-consistent filters (the variations are quite well captured); b) the inverse problem is well-posed but up to a multiplicative factor (see Section 5.3).

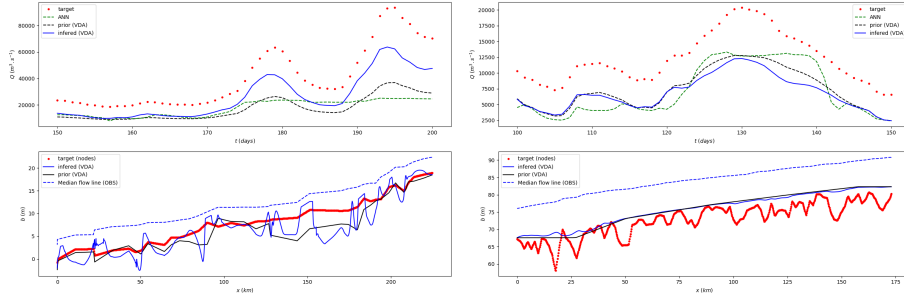


**Figure 12.** Discharge estimations for 2 rivers (randomly chosen) belonging to  $Q$ -Vset-out. (Left column) Jamuna. (Right column) Mississippi downstream.

(Up) Discharge values  $Q_{in}(t)$  vs time during the assimilating period only. (Down) Bathymetry values  $b(x)$  and the observed median flow line  $Z_{med}^{(obs)}(x)$ .

Let us recall again that one should generally be able to classify rivers by (rough) classes in terms of mean discharge from eg. the GRADES database, Lin et al. (2019). As a consequence, for a majority of rivers portions, one should be able to perform the estimations within the learning partition and not outside, like it is done here.

### 6.3.2 Estimations from a re-scaled prior

As previously discussed, the inverse problem based on the flow model without prior information is intrinsically ill-posed: one can estimate the space-time variations of the discharge values but up to a bias only, see Section 5.3. The numerical results obtained for rivers outside the learning range illustrate this feature, see Fig. 12 (see also Larnier et al. (2020a)). The knowledge of a mean value of  $Q$  (e.g. annual) would solve this bias issue. To illustrate this statement, the same numerical experiments as the previous ones are conducted excepted that the prior is  $2Q^{(ANN)}$  instead of  $Q^{(ANN)}$ . (The multiplicative factor 2 is chosen as a simple and roughly correct re-scaling; it does not correspond to any precise mean value of  $Q$ ). The obtained discharge estimations are plotted in Fig. 13 (“prior (VDA)” denotes  $Q_{in,p}^{(0)}$ ); performance criteria are indicated in Tab. 4.

As expected, the global estimations are much better, see Tab. 4; also the variations are well captured by the physically-based estimations (on contrary to the purely ANN-based ones). However, surprisingly in the Jamuna case, the VDA degrades the first guess estimations (“prior (VDA)”); on the opposite in the Mississippi case, the VDA improves the first guess estimation. However in all cases, the obtained nRMSE seems to be at least among the best ones existing up to now, see Frasson et al. (Submitted).

In conclusion these results confirm that for fully ungauged rivers (without any prior information, even not a rough mean value), the estimations can present a important bias but capture accurately the time discharge variations. And if any mean value of  $Q$  is known (e.g. annual) then the estimations become accurate with nRMSE very likely less than 30%.

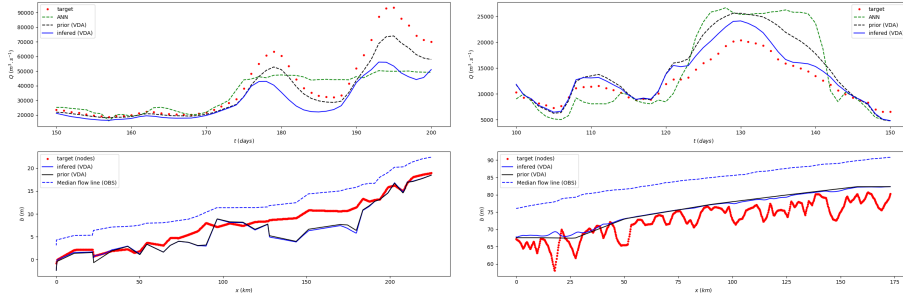


**Figure 13.** Discharge estimations for 2 rivers belonging to  $Q$ -Vset-out computed by VDA from the prior  $Q^{(ANN)}$  multiplied by 2. Discharge values  $Q_{in}(t)$  vs time during the assimilating period only. (Left column) Jamuna. (Right column) Mississippi downstream.

**On the robustness of the estimations in presence of noise.** Let us recall that the accuracy of  $Q^{(ANN)}$  is not affected if having less frequent data (eg. a few days period), since the employed input data of the ANN are non correlated (see the previous discussion). Moreover, the accuracy of  $Q^{ANN}$  is affected but reasonably if considering noisy SW measurements (with realistic Gaussian noises), see Section 3.4. As a consequence, one can expect that the VDA process propagate these errors but with the same order of magnitude (without importantly amplifying them). Indeed, sensitivity analyses (inversions robustness) performed to obtain the results presented in Brisset et al. (2018); Tuozzolo et al. (2019); Larnier et al. (2020a); Frasson et al. (Submitted), both for the algebraic flow model and the VDA algorithm, have demonstrated a good robustness with respect to the WS measurement errors. Indeed, as already mentioned, the greatest origin of the errors is from far the bias, therefore due to the inaccuracy of the first guess. Recall that the VDA enables to capture well the space-time *variations* of the flow (at the hours scale around the observation instant), Brisset et al. (2018); Tuozzolo et al. (2019); Larnier et al. (2020a); Frasson et al. (Submitted).

## 7 Estimations from newly acquired data

Given a river portion, the VDA, process enables the calibration of flow models: the river has been “learned”. In particular, the estimation of an effective bathymetry  $b(x)$  (equivalently  $A_0(x)$ ) is available. Next, given newly acquired WS measurements, three discharge estimators may be employed: the trained ANN (Section 3), the algebraic flow model (5) and the calibrated flow model (B1).

If the newly acquired data belong to the learning values ranges (in terms of  $(Z, W)$  values) then either the ANN or the dynamic flow model (B1) with  $Q_{in}(t)$  identified by VDA may be satisfactorily employed. Note that the model (B1) is a-priori more accurate than the ANN model since physically consistent, see Section 6.2 for an illustration of this feature. Moreover (B1) enables space-time extrapolation of discharge outside the measurements locations; this is not possible if using the ANN

630 model. However a particularly interesting alternative is to employ the “low cost” algebraic flow model (5). This is what is illustrated in this section.

## 7.1 Estimations based on the algebraic flow model

Given newly acquired data, a strategy to estimate  $Q$  in real computational time can be as follows.

- *Step 1) Recalibration of the friction coefficient  $K$ .*  
 635 Given  $(Q_{r,p}^{(VDA)}, A_{0,r}^{(VDA)})$  obtained after the VDA process, the algebraic model (5) is solved to obtain  $(\alpha_r, \beta_r)^{(LF)}$ . This computation provides the effective low-Froude friction parameter  $K_{r,p}^{(LF)}$ ;  $K_{r,p}^{(LF)} = K((\alpha_r, \beta_r)^{(LF)}, A_{0,r}; Z_{r,p})$ , see (4).
- *Step 2) Estimation from newly acquired data using the algebraic flow model (5).*  
 640 Given  $(A_{0,r}^{(VDA)}, (\alpha_r, \beta_r)^{(LF)}) \forall r$ , given new WS measurements  $(Z_{r,p}, W_{r,p}, S_{r,p})_{R,P+1}$ , the coefficients  $(c_{r,p}^{(k)})$ ,  $k = 1, 2, 3$ , and  $c_r^{(4)}$  in (5) can be evaluated. Then, the estimation  $Q_{r,p}^{(RT)}$ ,  $\forall r \forall p$ , can be explicitly obtained from (5), therefore computed in real time.

*Remark.* No uncertainty envelope on  $Q^{(RT)}$  is presented because of the necessarily arbitrary choices if doing so. Indeed, one could easily present uncertainties as follows. At Step 1), one can introduce an uncertainty model on  $Q^{(VDA)}$  by considering it as a random variable e.g.  $Q^{(VDA)} \sim \mathcal{N}(\bar{Q}^{(VDA)}, \sigma_Q)$ . Then if using the Metropolis-Hasting algorithm to compute the effective  
 645 Low-Froude values  $(\alpha, \beta)_r^{(LF)}$ , one obtains  $K_{r,p}$  as a random variable with a corresponding standard deviation  $\sigma_K$ . Next at Step 2), the “Real-Time” estimation denoted by  $Q_{r,p}^{(RT)}$  (explicit solution of (5)) is a random variable with a corresponding standard deviation  $\sigma_{final}$ . Therefore by setting a priori uncertainty on the pdf of  $Q^{(VDA)}$  and  $K_r$  (or  $(\alpha, \beta)_r$  e.g. as in Section 4.3 with  $\mathcal{U}(10, 100)$  for  $\alpha_r$ ,  $\mathcal{N}(0, 0.3)$  for  $\beta_r$ ), we can obtain the resulting uncertainty on  $Q^{(RT)}$ .

## 7.2 Numerical results

650 The VDA estimations in Section 6 have been obtained from relatively short time periods compared to a complete year, see Tab. 5; however the chosen periods are relatively representative of the potential annual variations. These “VDA periods” are the “calibration” (or “learning”) periods. Outside these calibration periods, the WS measurements are considered as newly acquired; then, the real-time discharge  $Q^{(RT)}$  is estimated as described in the previous paragraph. Moreover the real-time estimation  $Q^{(RT)}$  is computed for the calibration period too, see Fig. 14. This enables to compare  $Q^{(RT)}$  with  $Q^{(target)}$  for  
 655 all periods. For the two rivers outside the learning partition  $Q$ -Lset (Jamuna and Mississippi downstream), the prior value is  $2Q^{(ANN)}$  and not  $Q^{(ANN)}$ . The discharge estimations are plotted in Fig. 13. In the calibration periods, the estimation  $Q^{(RT)}$  differs from  $Q_{in,p}^{(0)}$  (“prior VDA”) because of the use of the bathymetry estimation obtained after VDA. Performance criteria are indicated in Tab. 5.

Again for the rivers belonging to the learning partition (Garonne downstream, Ohio) therefore with an already excellent  
 660 estimation by ANN, all the estimations are accurate (17-28% nRMSE). For the rivers (far) outside the learning partition (Jamuna and Mississippi downstream), the nRMSE remains good (21 – 35%), equal to the order of magnitude of the errors

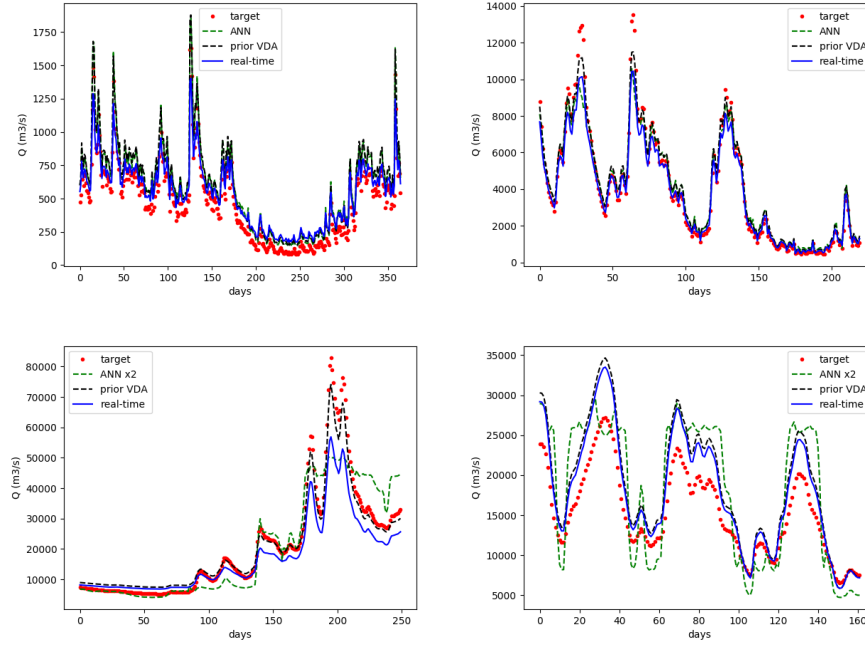


**Figure 14.** Real-time discharge estimations  $Q(t)$  vs time during the complete time period by solving (5). “Prior” corresponds to the first guess  $Q_{in,p}^{(0)}$  presented in Section 4.3.

(Up)(L) Garonne downstream. (Up)(R) Ohio.

(Down) (L) Jamuna. (Down)(R) Mississippi downstream.

River name	Calibration period (days)	Complete estimation period (days)	nRMSE	NSE
Garonne downstream	[120-170]	[1-365]	28.6 %	0.78
Ohio	[1-50]	[1-220]	17.3 %	0.95
Jamuna	[150-200]	[1-250]	35.0 %	0.84
Mississippi downstream	[100-150]	[1-162]	21.8 %	0.61

**Table 5.** The calibration periods are those considered in the VDA processes. The performance scores are those obtained for  $Q^{(RT)}$  during the complete period.

when measuring discharges. In these two cases, the real-time estimation (which physically-based) is better than the purely data-driven prior  $2Q^{(ANN)}$ . However, it can be noticed that  $Q^{(RT)}$  (solution of a re-run after the VDA calibration) may be better or worse than the prior VDA  $Q_{in}^{(0)}$ . However, again in all cases the obtained nRMSE is at least among the best ones existing up to now for ungauged rivers, Frasson et al. (Submitted); moreover these estimations are computed in real-time given newly acquired WS measurements.

## 8 Conclusions

This study proposes the first combined deep learning - data assimilation approach to infer river discharge values from altimetry measurements only (here synthetic SWOT like data with 1 day repeat). The resulting algorithm, named HiVDI (Hierarchical Variational Discharge Inference), is an important improvement of the former version presented in Larnier et al. (2020a); Frasson et al. (Submitted). The considered data are synthetic flow observations generated from outputs of various calibrated flow models for 29 rivers portions available in the reference Pepsi 1 and 2 datasets, Durand et al. (2016); Frasson et al. (Submitted)). The only ancillary data of the method is a local drainage area extracted from the HydroSHEDS dataset Lehner et al. (2008). The elaborated algorithm relies on: a deep neural network providing a first estimation of  $Q$  which is next improved by a low Froude flow model (algebraic flow model). The resulting discharge estimation is good for ungauged rivers at the "SWOT reach scale" (SwReachSc) if presenting discharge values within the learning partition ( $\approx 20 - 40\%$  nRMSE with the present perfect data). For river discharges outside the learning partition, the time variations are very well captured but a bias remains; this bias is inherent to the automatic learning approach. However, one should generally be able to classify rivers by (rough) classes in terms of mean discharge from eg. the GRADES database, Lin et al. (2019). As a consequence, for a majority of rivers portions, one should be able to perform the estimations within the learning partition and not outside. Since the employed input data are non correlated, neither in space nor in time, the accuracy is not affected if considering less frequent data (eg with a few days frequency).

Next, an advanced Variational Data Assimilation (VDA) method enables the estimation of accurate space-time variations of  $Q(x, t)$  for any location and any time at fine scale; however the potential bias may remain. It is mathematically shown that this bias cannot be removed if defining the estimations by inverting the classical hydro models only. However any mean value of  $Q$  (eg. seasonal or annual) enables to remove the bias, therefore providing accurate estimations. In short, the estimation is based on automatic learning and the inversion of two hierarchical flow models. Given a representative WS measurements set (eg. during a complete year), the method results on two calibrated flow models of hierarchical complexity (algebraic and ) for each river portion. Next, given newly acquired WS measurements, the algebraic flow model is accurate enough ( $\approx 15 - 35\%$  nRMSE for perfect data) and low-cost enough to provide in real time the estimation of  $Q$  at km scale and at the hours observation scale. The HiVDI algorithm is implemented into the open-source computational software DassFlow Larnier et al. (2020b). In forthcoming studies, this algorithm should be evaluated on the basis of the SWOT simulator data (considering both the Cal-Val orbit and the nominal orbit). Once these more advanced evaluations done, the HiVDI algorithm may be employed to estimate both discharge and bathymetry from the forthcoming SWOT datasets for ungauged or poorly gauged rivers.

### Appendix A: River geometries

Recall that the SWOT-like measurements consist in sets  $(Z_{r,p}, W_{r,p})_{R,P+1}$ . Moreover at SwReachSc, WS slopes values  $S_{r,p}$  are available and taken into account into the algebraic flow model (see next section). The values  $S_{r,p}$  are either deduced from the elevation values  $Z$  or estimated by an internal instrument process.

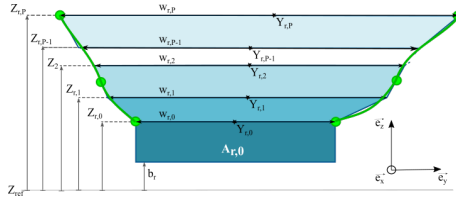


**Figure A1.** A cross section  $A_r$  is the superimposition of the observed trapeziums  $A_{r,p}$  defined from the  $p$ -ordered SWOT measurements  $(Z_{r,p}, W_{r,p})$  + the unobserved lowest cross-section  $A_0$ . Next, the shape is approximated by a cubic spline (green curve).

700 The considered river geometries are derived from the datasets  $(Z_{r,p}, W_{r,p})_{R,P+1}$ . The cross-sectional geometry consists in discrete cross sections formed by asymmetrical trapezium layers  $(Z_{r,p}, W_{r,p})$ , see Fig. A1. The cross-sectional areas  $A_{r,p}$  satisfy:  $A_{r,p} = A_{r,0} + \delta A_{r,p} = A_{r,0} + \int_{Z_{r,0}}^{Z_{r,p}} W_r(h) dh \quad \forall r \quad \forall p \geq 1$ .

The variations  $\delta A_{r,p}$  are approximated by the trapeziums:  $\delta A_{r,p} \approx \sum_{q=1}^p \frac{1}{2} (W_r^q + W_r^{q-1}) (h_r^q - h_r^{q-1})$ .

The lowest cross-sectional areas denoted by  $A_{r,0}$  ( $r = 1, \dots, R$ ) are unobserved; they are key unknowns of the flow models.  
 705 They can be represented by rectangles or any other fixed shape (e.g. a parabola); all the other cross-sectional areas are trapezoidal. Next, for simplicity and regularization purposes, the shape is approximated at a cubic spline curve in the least square sense (green curve), see Fig. A1.

For all considered rivers we have the hydraulic radius  $R^h$  which satisfies:  $R_{r,p}^h \approx h_{r,p}$ . Also since  $W \gg h$ , it follows the effective depth expression:  $h_{r,p} \approx (A_{r,0} + \delta A_{r,p})(W_{r,0} + W_{r,p})^{-1}$ .

## 710 Appendix B: The dynamic flow model

The considered dynamic flow model is the 1D Saint-Venant equations in their non conservative form in  $(A, Q)$  variables;  $A$  the wetted-cross section [ $m^2$ ],  $Q$  the discharge [ $m^3 \cdot s^{-1}$ ]. The equations read as follows, see e.g. Chow (1964)

$$\begin{cases} \partial_t A + \partial_x Q &= 0 \\ \partial_t Q + \partial_x \left( \frac{Q^2}{A} \right) + g A \partial_x Z &= -g A S_f(A, Q; K) \end{cases} \quad (\text{B1})$$

715

where  $g$  is the gravity magnitude [ $m \cdot s^{-2}$ ],  $Z$  is the WS elevation [ $m$ ],  $Z = (b + h)$  where  $b$  is the lowest rectangular cross-section (bed) level [ $m$ ] and  $h$  is the water depth [ $m$ ].

At inflow (upstream), the discharge  $Q_{in}(t)$  is imposed.

At outflow (downstream), if known the WS elevation  $Z_{out}$  is imposed. If unknown, the normal depth (based on the Manning-  
 720 Strickler equilibrium equation) is imposed. Recall that the normal depth depends on the prior values  $(K, A_0)$  at outflow.

The RHS term  $S_f$  is the classical Manning-Strickler friction term:  $S_f(A, Q; K) = \frac{|Q|Q}{K^2 A^2 R_h^{4/3}}$  with  $K$  the Strickler roughness coefficient [ $m^{1/3} \cdot s^{-1}$ ] with  $R_h \approx h$  [ $m$ ].  $K$  is defined following the local power-law (4). The discharge  $Q$  is related to the water velocity  $u$  [ $m \cdot s^{-1}$ ] by the relation:  $Q = uA$ .

This 1D Saint-Venant model is discretized using the classical implicit Preissmann scheme (see e.g. Cunge (1980)) with a  
725 space cell length  $\Delta x = 200\text{m}$  and time step  $\Delta t = 1\text{h}$ .

The numerical model has been implemented in the computational software DassFlow Larnier et al. (2020b).

*Author contributions.* J.M. has designed the research plan, the methods, equations and algorithms; he has written the manuscript. K.L. has implemented the algorithms and has performed the numerical results. Both authors have contributed to the results analysis and the methods selection.

730 *Acknowledgements.* K. Larnier, software engineer at CS group corp., has been funded by CNES. The authors would like to acknowledge Miss Ha Nhi Ngo, INSA 5th year student, which has provided a preliminary Jupyter - Python sheet facilitating the statistical analysis. The authors would like to acknowledge Renato Frasson (NASA/JPL) and Mike Durand (Univ. Ohio) for sharing Pepsi-2 dataset.

*Competing interests.* No competing interests are present.

## References

- Asch, M., Bocquet, M., and Nodet, M.: Data assimilation: methods, algorithms, and applications, vol. 11, SIAM, 2016.
- Biancamaria, S., Lettenmaier, D. P., and Pavelsky, T. M.: The SWOT Mission and Its Capabilities for Land Hydrology, Surveys in Geophysics, 37, 307–337, 2016.
- Bouttier, F. and Courtier, P.: Data assimilation concepts and methods March 1999, Meteorological training course lecture series. ECMWF, p. 59, 2002.
- Brisset, P., Monnier, J., Garambois, P.-A., and Roux, H.: On the Assimilation of Altimetric Data in 1D Saint-Venant River Flow Models, Adv. Water Res., 119, 41–59, 2018.
- Chen, L. and Wang, L.: Recent advance in earth observation big data for hydrology, Big Earth Data, 2, 86–107, 2018.
- Chow, V.: Handbook of applied hydrology, McGraw-Hill Book Co., New-York, 1467 pages, 1964.
- Cunge, J.: Practical aspects of computational river hydraulics, Pitman Publishing Ltd. London,(17 CUN), 1980, 420, 1980.
- Dalcín, L., Paz, R., and Storti, M.: MPI for Python, Journal of Parallel and Distributed Computing, 65, 1108–1115, 2005.
- Durand, M., Gleason, C., Garambois, P.-A., Bjerklie, D., Smith, L., Roux, H., Rodriguez, E., Bates, P., Pavelsky, T., Monnier, J., et al.: An intercomparison of remote sensing river discharge estimation algorithms from measurements of river height, width, and slope, Water Resources Research, 2016.
- Frasson, R., Durand, M., Larnier, K., Gleason, C., Andreadis, K., Hagemann, M., Dudley, R., Bjerklie, D., Oubanas, H., Garambois, P.-A., Malaterre, P.-O., Lin, P., Pavelsky, T., and Monnier, J.: Exploring the factors controlling the performance of the Surface Water and Ocean Topography mission discharge algorithms, Submitted.
- Garambois, P.-A. and Monnier, J.: Inference of effective river properties from remotely sensed observations of water surface, Advances in Water Resources, 79, 103–120, 2015.
- Garambois, P.-A., Larnier, K., Monnier, J., Finaud-Guyot, P., Verley, J., Montazem, A., and Calmant, S.: Variational inference of effective channel and ungauged anabranching river discharge from multi-satellite water heights of different spatial sparsity, Journal of Hydrology, 581, 124 409, 2020.
- Glorot, X., Bordes, A., and Bengio, Y.: Deep sparse rectifier neural networks, in: Proceedings of the fourteenth international conference on artificial intelligence and statistics, pp. 315–323, 2011.
- Gore, J. A. and Banning, J.: Discharge measurements and streamflow analysis, in: Methods in Stream Ecology, Volume 1, pp. 49–70, Elsevier, 2017.
- Haben, S., Lawless, A., and Nichols, N.: Conditioning and preconditioning of the variational data assimilation problem, Computers & Fluids, 46, 252–256, 2011a.
- Haben, S., Lawless, A., and Nichols, N.: Conditioning of incremental variational data assimilation, with application to the Met Office system, Tellus A, 63, 782–792, 2011b.
- Hascoët, L. and Pascual, V.: The Tapenade Automatic Differentiation tool: Principles, Model, and Specification, ACM Transactions On Mathematical Software, 39, 2013.
- Kaltenbacher, B., Neubauer, A., and Scherzer, O.: Iterative regularization methods for nonlinear ill-posed problems, vol. 6, Walter de Gruyter, 2008.
- Kanevski, M., Pozdnoukhov, A., Pozdnukhov, A., and Timonin, V.: Machine learning for spatial environmental data: theory, applications, and software, EPFL press, 2009.

- Kingma, D. and Ba, J.: Adam: A method for stochastic optimization, arXiv preprint arXiv:1412.6980, 2014.
- Larnier, K., Monnier, J., Garambois, P. A., and Verley, J.: River discharge and bathymetry estimation from SWOT altimetry measurements, *Inverse Problems in Sciences and Engineering*, p. ( <https://doi.org/10.1080/17415977.2020.1803858> ), 2020a.
- Larnier, K., Monnier, J., et al.: Data Assimilation for Free Surface Flows, Tech. rep., Mathematics Institute of Toulouse - INSA - CNES -  
775 CNRS - CS group, <http://www.math.univ-toulouse.fr/DassFlow>, 2020b.
- LeCun, Y., Bengio, Y., and Hinton, G.: Deep learning, *nature*, 521, 436, 2015.
- Lehner, B., Verdin, K., and Jarvis, A.: New Global Hydrography Derived From Spaceborne Elevation Data, *Eos, Transactions American Geophysical Union*, 89, 93–94, <https://doi.org/10.1029/2008EO100001>, <https://agupubs.onlinelibrary.wiley.com/doi/abs/10.1029/2008EO100001>, 2008.
- 780 Lin, P., Pan, M., Beck, H. E., Yang, Y., Yamazaki, D., Frasson, R., David, C. H., Durand, M., Pavelsky, T. M., Allen, G. H., et al.: Global reconstruction of naturalized river flows at 2.94 million reaches, *Water resources research*, 55, 6499–6516, 2019.
- Lorenc, A., Ballard, S., Bell, R., Ingleby, N., Andrews, P., Barker, D., Bray, J., Clayton, A., Dalby, T., Li, D., et al.: The Met. Office global three-dimensional variational data assimilation scheme, *Quarterly Journal of the Royal Meteorological Society*, 126, 2991–3012, 2000.
- Lorenc, A. C.: Optimal nonlinear objective analysis, *Quarterly Journal of the Royal Meteorological Society*, 114, 205–240, 1988.
- 785 Mallat, S.: Understanding deep convolutional networks, *Philosophical Transactions of the Royal Society A: Mathematical, Physical and Engineering Sciences*, 374, 20150203, 2016.
- Monnier, J.: Variational data assimilation and model learning, Open Online Advanced Course, INSA Toulouse, 2020.
- Monnier, J. and Zhu, J.: Inference of the bottom topography in anisothermal mildly-sheared shallow ice flows, *Computer Methods in Applied Mechanics and Engineering*, 348, 954–977, 2019.
- 790 Oubanas, H., Gejadze, I., Malaterre, P.-O., Durand, M., Wei, R., Frasson, R. P. M., and Domeneghetti, A.: Discharge Estimation in Ungauged Basins Through Variational Data Assimilation: The Potential of the SWOT Mission, *Water Resources Research*, 54, 2405–2423, 2018a.
- Oubanas, H., Gejadze, I., Malaterre, P.-O., and Mercier, F.: River discharge estimation from synthetic SWOT-type observations using variational data assimilation and the full Saint-Venant hydraulic model, *Journal of Hydrology*, 559, 638–647, 2018b.
- Paiva, R. C., Durand, M. T., and Hossain, F.: Spatiotemporal interpolation of discharge across a river network by using synthetic SWOT  
795 satellite data, *Water Resources Research*, 51, 430–449, 2015.
- Pujol, J., Garambois, P.-A., Finaud-Guyaot, P., Monnier, J., Larnier, K., Mose, R., Biancamaria, S., Yesou, H., Moreira, D., Paris, A., and Calmant, S.: Estimation of Multiple Inflows and Effective Channel by Assimilation of Multi-satellite Hydraulic Signatures: The Ungauged Anabranching Negro River, *Journal of Hydrology*, 2020.
- Rodriguez, E. and Esteban-Fernandez, D.: The surface water and ocean topography mission (SWOT): The Ka-band Radar Interferometer  
800 (KaRIn) for water level measurements at all scales, in: *Sensors, Systems, and Next-Generation Satellites XIV*, vol. 7826, p. 782614, International Society for Optics and Photonics, 2010.
- Rodriguez, E. et al.: SWOT science requirements document, JPL document, JPL, 2012.
- Schwatke, C., Dettmering, D., Bosch, W., and Seitz, F.: DAHITI—an innovative approach for estimating water level time series over inland waters using multi-mission satellite altimetry, *Hydrology and Earth System Sciences* 19 (10): 4345–4364, 2015.
- 805 Tarantola, A.: Inverse problem theory and methods for model parameter estimation, vol. 89, SIAM, 2005.
- Tarpanelli, A., Santi, E., Tourian, M. J., Filippucci, P., Amarnath, G., and Brocca, L.: Daily river discharge estimates by merging satellite optical sensors and radar altimetry through artificial neural network, *IEEE Transactions on Geoscience and Remote Sensing*, 57, 329–341, 2018.

- Tuozzolo, S., Lind, G., Overstreet, B., Mangano, J., Fonstad, M., Hagemann, M., Frasson, R., Larnier, K., Garambois, P.-A., Monnier, J., and  
810 Durand, M.: Estimating river discharge with swath altimetry: A proof of concept using AirSWOT observations, *Geophysical Research  
Letters*, 46, 1459–1466, 2019.
- Yamazaki, D., O’Loughlin, F., Trigg, M. A., Miller, Z. F., Pavelsky, T. M., and Bates, P. D.: Development of the global width database for  
large rivers, *Water Resources Research*, 50, 3467–3480, 2014.